Central histaminergic system reduces response gain and slows visual processing in the retina and lateral geniculate nucleus of awake mice

Authors: Matteo Tripodi[1], Hiroki Asari*[1]

Affiliations:

1. Epigenetics and Neurobiology Unit, EMBL Rome, European Molecular Biology Laboratory, Monterotondo, 00015, Italy

***Corresponding author:** Hiroki Asari, E-mail: asari@embl.it

Author contributions: M.T. and H.A. designed the study; M.T. performed experiments; M.T. and H.A. analyzed the results; and M.T. and H.A. wrote the manuscript.

Competing interests: The authors declare no competing financial interests.

Key words: retinal ganglion cells; lateral geniculate nucleus; histaminergic modulation; tuberomammillary nucleus.

Acronyms: AAV, adeno-associated virus; ANOVA, analysis of variance; DLP, digital light processing; DRN, dorsal raphe nucleus; HDC, histidine decarboxylase; GABA, γ-aminobutyric acid; IQR, interquartile range; IR, infrared; LED, light emitting diode; LGN, lateral geniculate nucleus; OT, optic tract; PFA, paraformaldehyde; PSAM/PSEM, pharmacologically selective actuator/effector module; RF, receptive field; RGC, retinal ganglion cell; STA, spike-triggered average; t-SNE, t-distributed Stochastic Neighbor Embedding; UV, ultraviolet.

Abstract

Sensory processing is dynamically modulated by an animal's behavior and internal states. Growing evidence suggests that such modulation starts from early stages, already at the retina, but the underlying mechanisms remain elusive. Combining pharmacological and chemogenetic tools with single-unit extracellular recordings in awake head-fixed mice, here we identified that the visual responses of retinal ganglion cells and the lateral geniculate nucleus were both made weaker and slower by histaminergic projections from the tuberomammillary nucleus of the posterior hypothalamus. The observed changes in the visual responses were, however, not directly linked with histaminergic modulation of pupil dynamics or locomotion behavior. Instead, our computational modelling analysis suggests that the temporal response modulations arise from changes in the intrinsic properties of the circuit, such as gain modulation via the histamine H1 receptors in the retina. Facilitation of visual processing at low histamine levels may offer an ethological advantage, enabling animals to respond rapidly to visual threats during periods of reduced activity.

Introduction

In the mammalian brain, histaminergic neurons are exclusively located in the tuberomammillary nucleus (TMN) and surrounding areas of the posterior hypothalamus (Haas and Panula, 2003). They express histidine decarboxylase (HDC) and innervate widely across the brain (Lin et al., 2023), including the retina (Gastinger et al., 1999; Repérant et al., 2007; Greferath et al., 2009; Warwick et al., 2024). These neurons remain silent during sleep, but increase their firing during wakefulness and reach their maximal activity at the state of high vigilance, much as other monoaminergic systems do, such as the serotonergic neurons in the dorsal raphe nucleus (DRN) of the brain stem (Lin et al., 2023; Takahashi et al., 2006; Thakker, 2011). Brain histamine exerts its effects on neurons via three types of receptors: the H1 and H2 receptors mediate excitation of postsynaptic cells, while the H3 receptors serve as an auto-receptor to presynaptically inhibit histamine release (Haas and Panula, 2003). The role of the H4 receptors in the central nervous system remains unknown (Strakhova et al., 2009). The

central histaminergic system has been implicated in regulating an animal's internal state and a broad range of behavior, including the sleep-wake cycle (John et al., 2004; Mochizuki et al., 1992), arousal (Parmentier et al., 2002; Scammell et al., 2018), suppression of food intake (Khouma et al., 2023; Valdés et al., 2010; Wang et al., 2015) and learning (Kamei et al., 1993; Klapdor et al., 1994; Orsetti et al., 2001; Rubio et al., 2002). Histaminergic neurons, however, corelease γ-aminobutyric acid (GABA) and interact with other neuromodulatory systems, such as the cholinergic and serotonergic systems (Khateb et al., 1995; Brown et al., 2002; Lin et al., 2023). This makes it difficult to dissect the effects of histamine by itself on neural circuit functions. In particular, histaminergic modulation of sensory processing remains largely elusive (Lee and Dan, 2012; McCormick et al., 2020).

The retina performs the first stage of visual processing, and conveys visual information to the brain via spike trains of retinal ganglion cells (RGCs). Growing evidence supports that the activity of RGCs is correlated with various behavioral measures, such as locomotion and pupil size (Schröder et al., 2020; Liang et al., 2020; Reggiani et al., 2023; Boissonnet et al., 2023), pointing to a more dynamic role of the retina than is assumed for a deterministic processor. The vertebrate retina is part of the central nervous system equipped with both intrinsic and extrinsic neuromodulation mechanisms, much as other brain regions are (Lee and Dan, 2012; McCormick et al., 2020). For instance, dopamine is synthesized and released by a group of retinal amacrine cells under the control of circadian rhythm, and contributes to adjusting the retinal circuitry for rod or cone vision by modulating gap-junction couplings (Bloomfield and Völgyi, 2009). Such retinal intrinsic mechanisms of neuromodulation are, however, much slower than needed to modulate retinal function to follow rapid behavioral changes (Jacoby et al., 2018; Goel and Mangel, 2021). To this end, the retina seems to exploit the centrifugal system to receive inputs from a variety of brain regions in a species-specific manner (Repérant et al., 2007). For example, histaminergic and serotonergic projections from TMN and DRN, respectively, have been anatomically described in the mammalian retina (Gastinger et al., 1999; Greferath et al., 2009; Labandeira-Garcia et al., 1990; Warwick et al.,

2024). However, compared to the isthmo-optic pathway in birds (Wilson and Lindstrom, 2011) or the olfacto-retinal circuit in fish (Esposti, et al., 2013), little is known about the function of the mammalian centrifugal system (Vereczki et al., 2024).

Combining in vivo single-unit extracellular recordings from either the lateral geniculate nucleus (LGN) or the optic tract (OT) with pharmacological and chemogenetic tools, here we explored how histamine affects the early visual processing in awake head-fixed mice. During the recording sessions, we simultaneously monitored the subject animal's behavior, such as pupil dynamics and locomotion, to better correlate the effects of histamine on the visual response properties with those on the behavioral measures. We also took a computational approach to clarify the net effect of histamine on the visual responses from functional viewpoints. Because visual processing in the brain fully relies on the signals from the retina, characterization of the retinal operation in vivo is indispensable to better understand how the visual system works.

Results

Histamine leads to weaker and slower visual responses in the mouse lateral geniculate nucleus

To investigate how histamine influences the mouse visual system, we first performed in vivo single-unit extracellular recordings from the lateral geniculate nucleus (LGN) in awake head-fixed mice (Figure 1A,B and Supplementary Figure 1), and compared the visual response properties of the recorded cells before and after perturbing the central histaminergic system (Figures 1 and 2; see Methods for details). Besides directly examining the responses to repeatedly presented visual stimuli, we employed stimulus ensemble statistical techniques ("reverse correlation") to systematically characterize the visual response properties of the recorded cells in the framework of a linear-nonlinear cascade model (Boissonnet et al., 2023). In particular, using full-field white-noise stimuli, we analyzed histaminergic effects on 1) the linear temporal filter, estimated by the spike-triggered average (STA) stimulus – i.e., the mean

81 stimulus that triggered spiking responses – under a given behavioral state; and 2) the static
82 nonlinear gain function, i.e., an instantaneous mapping of the STA output to the neural
83 responses (Figure 2B). We also functionally mapped the receptive field (RF) of the cells by
84 calculating the linear spatial filter from their responses to random binary "checkerboard" stimuli,
85 where the contrast of each spatial location was randomly and independently inverted over
86 time. To manipulate the histaminergic system, we used two different approaches
87 (Supplementary Figure 2). The first was the chemogenetic activation of the central
88 histaminergic system (Magnus et al., 2011). We injected Cre-dependent adeno-associated
89 viruses (AAVs) carrying pharmacologically selective actuator module (PSAM)-5HT3HC
90 channels into the tuberomammillary nucleus (TMN) of the posterior hypothalamus in histidine
91 decarboxylase (HDC)-Cre transgenic mice, and then achieved selective activation of the
92 target neurons by systemic administration of the pharmacologically selective effector molecule
93 (PSEM; 5mg/kg). The second approach was the use of pharmacological tools in wild-type
94 mice (Figure 1C; Thakkar, 2011). Specifically, we used chlorphenamine (5 mg/kg; Frisch et
95 al., 1997; Valle-Baurista et al. 2022), an antagonist of a postsynaptic histamine receptor H1;
96 and ciproxifan (12 mg/kg; Browman et al., 2004; Muindi et al., 2015), an antagonist of the H3
97 auto-receptor that presynaptically inhibits histamine release. These drugs effectively down-
98 and up-regulate the action of histamine in the nervous system, respectively. Thus, resulting
99 changes in visual processing, if any, were expected to be in opposite directions. While we let
100 the animals move freely under the head-fixed condition, the reverse correlation analysis was
101 done on the periods when the animals stayed stationary (<2 cm/s) to minimize the side effect
102 of locomotion behavior (Supplementary Figure 3; Erisken et al., 2014; Schröder et al., 2020).

103 Upon chemogenetically activating HDC+ neurons in TMN, we found that LGN neurons
104 generally showed weaker and slower visual responses. The peak responses to stimulus onset
105 and offset were both significantly reduced in amplitude and prolonged in latency (Figure 1D-
106 F). Moreover, the mean firing rate during the white-noise visual stimulation became
107 significantly lower (median, -4.7 Hz; interquartile range (IQR), 7.9 Hz; $p<0.001$, Wilcoxon

signed-rank test here and thereafter unless otherwise noted; n=52 from 3 animals); and the response gain also significantly decreased (median, -33%; IQR, 55%; p<0.001) that we computed as the ratio of the estimated static nonlinearity functions before and after PSEM injection (Figure 2C,G). The temporal filter became elongated regardless of their functional cell types (Supplementary Figure 4), leading to significantly longer peak latencies (median, +31 ms; IQR, 33 ms; p<0.001) and lower peak frequencies (median, -16%; IQR, 47 %; p<0.001).

Consistent results were obtained when histamine release was pharmacologically up-regulated. Specifically, after the application of ciproxifan (H3 antagonist), both the onset and offset peak responses became weaker and longer (Figure 1G-I). Furthremore, during white-noise sitmulation, we found significantly reduced mean firing rates (median, -3.0 Hz; IQR, 5.5 Hz; p<0.001; n=126 cells from 4 animals) and response gain (median, -23%; IQR, 65%; p=0.002); and the linear temporal filters showed significantly longer peak latency (median, +16 ms; IQR, 11 ms; p<0.001) and lower peak frequency (median, -39%; IQR, 20%; p=0.08; Figure 2D,H). These effects of the pharmacological treatment were less prominent than those of the chemogenetic manipulation (Figures 1P,Q and 2K-N). None of these treatments significantly affected the estimated RF size at the population level (Supplementary Figure 5).

In contrast, chlorphenamine (H1 antagonist) led to marginal changes in the visual response properties of LGN neurons in the opposite direction. The onset/offset stimulus responses were faster in some cells, but the changes were not statistically significant at the population level (Figure 1J-L). Likewise, we observed a tendency towards an increased mean evoked firing rate (median, +1.1 Hz; IQR, 6.8 Hz; p=0.09; n=110 cells from 3 animals) and response gain (median, +14%; IQR, 94%; p=0.015), and facilitated response kinetics with significantly higher peak frequency of the linear temporal filter (median, +4%; IQR, 15%; p=0.02) but no significant changes in its peak latency (median, 0 ms; IQR, 5 ms; p=0.7) or the RF size (Supplementary Figure 5). Taken together, these results indicate that histamine reduces the response gain and slows down the response kinetics in the mouse LGN.

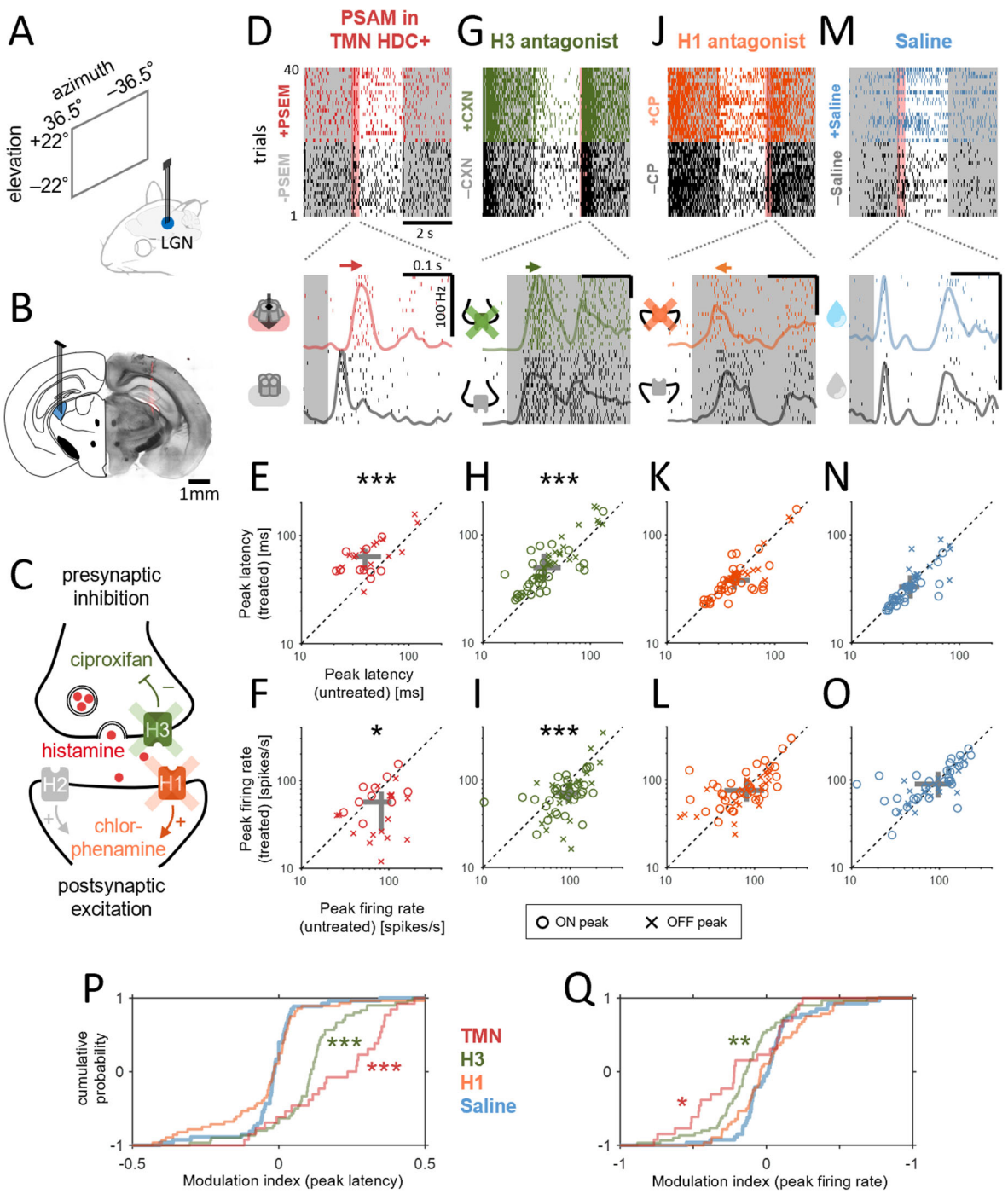

Figure 1: Histamine reduced LGN visual responses in awake head-fixed mice. *A,B*: schematic diagram of LGN recordings (A) and a representative histological image showing the electrode location (B; DiI stain, red). *C*: schematic diagram of histamine receptor localizations and their cellular function. Chlorphenamine blocks the postsynaptic receptor H1 (orange) that mediates the action of histamine postsynaptically, while ciproxifan blocks the autoreceptor H3 (green) that inhibits presynaptic histamine release. *D*: visual responses of a representative LGN cell to full-field contrast-inverting stimuli (2 s intervals) before and after chemogenetically activating HDC+ cells in TMN: *top*, spike raster across trials; *bottom*, zoom-in of the spike raster around stimulus onset (-50 ms to 250 ms, red shade on top) and peri-stimulus time histogram, showing a delay of the onset response after the chemogenetic treatment. *E,F*: pairwise comparison of the LGN population responses before and after the chemogenetic treatment (E, peak latency: untreated, 39±17 ms, median ± median absolute deviation; treated, 64±20 ms; p<0.001, Wilcoxon signed-rank test with Bonferroni correction;

F, peak firing rate: untreated, 82±33 Hz; treated, 57±26 Hz; p=0.04, n=26 LGN cells from 3 animals): circle, ON peak; cross, OFF peak; gray, inter-quartile range. *G-I*: corresponding data before and after ciproxifan administration (G, representative cell's response, with a zoom-in around stimulus offset; H, peak latency: 37±22 ms versus 50±26 ms, p<0.001; I, peak firing rate: 95±35 Hz versus 71±31; p<0.001, n=60 LGN cells from 4 animals). *J-L*: corresponding data before and after chlorphenamine administration (J, representative cell's response; K, peak latency: 42±20 ms versus 38±16 ms, p=0.3; L, peak firing rate: 81±43 Hz versus 76±33; p=0.5, n=56 LGN cells from 3 animals). *M-O*: corresponding data before and after saline administration (M, representative cell's response; N, peak latency: 35±22 ms versus 33±21 ms, p=0.2; O, peak firing rate: 97±48 Hz versus 89±34; p=0.5, n=53 LGN cells from 3 animals). *P,Q*: cumulative distributions of modulation indices before and after each treatment (in corresponding colors): P, peak latencies; Q, peak firing rate; *, p<0.05; **, p<0.01; ***, p<0.001 from the post-hoc test against the saline (control) condition on the average group ranks (Kruskal-Wallis test).

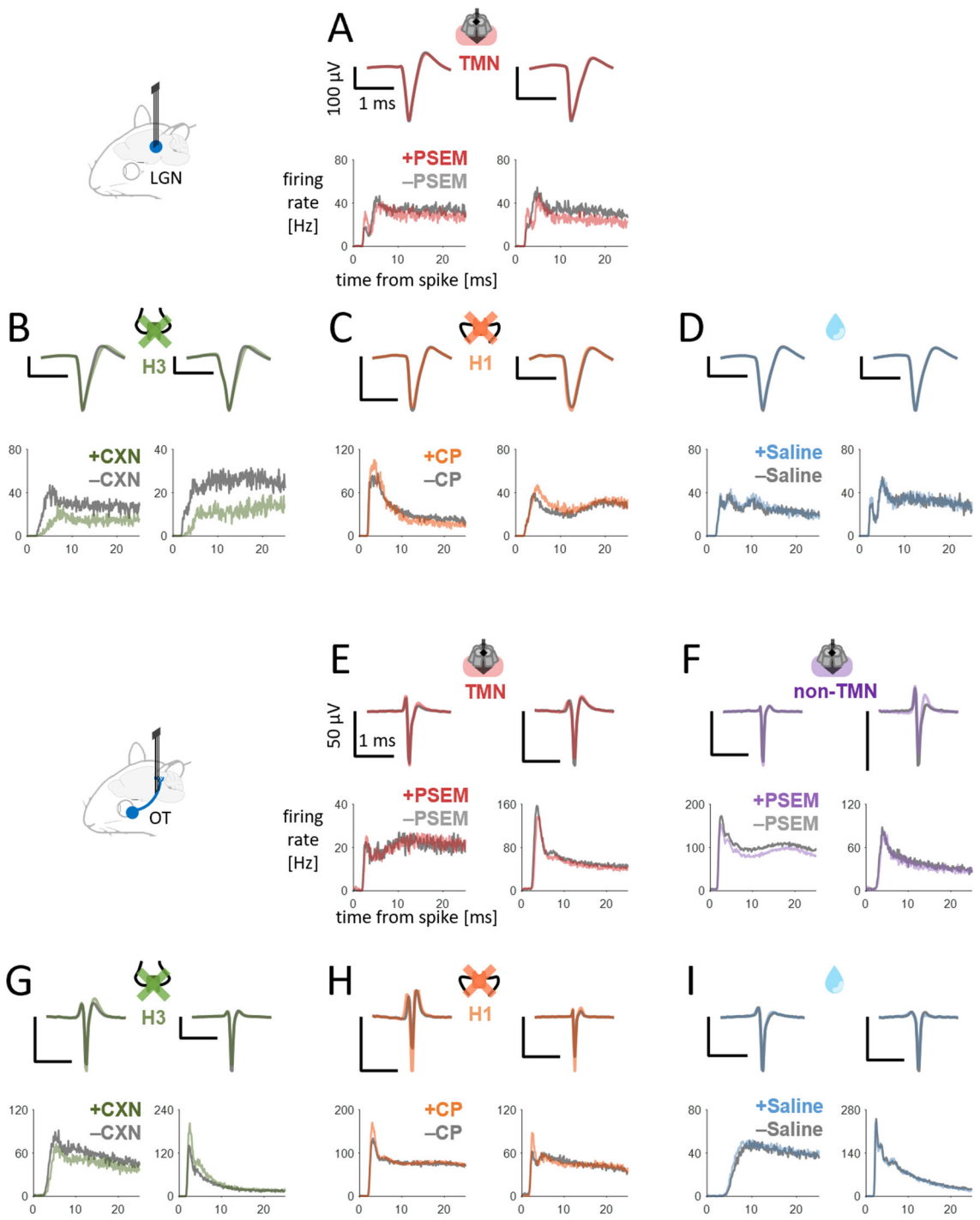

Supplementary Figure 1: spike waveform and autocorrelation of spike trains of representative cells across different conditions. *A*: average spike waveform (top) and auto-correlogram (bottom) of two representative LGN cells (left and right) before (black) and after (red) chemogenetic activation of TMN HDC+ cells. *B-D*: corresponding data for ciproxifan (B, green), chlorphenamine (C, orange), and saline administration (D, blue), each with two representative LGN cells. *E-I*: corresponding data for RGCs from optic tract recordings (E, chemogenetic activation of HDC+ cells in TMN; F, chemogenetic activation of HDC+ cells outside TMN; G, ciproxifan; H, chlorphenamine; I, saline).

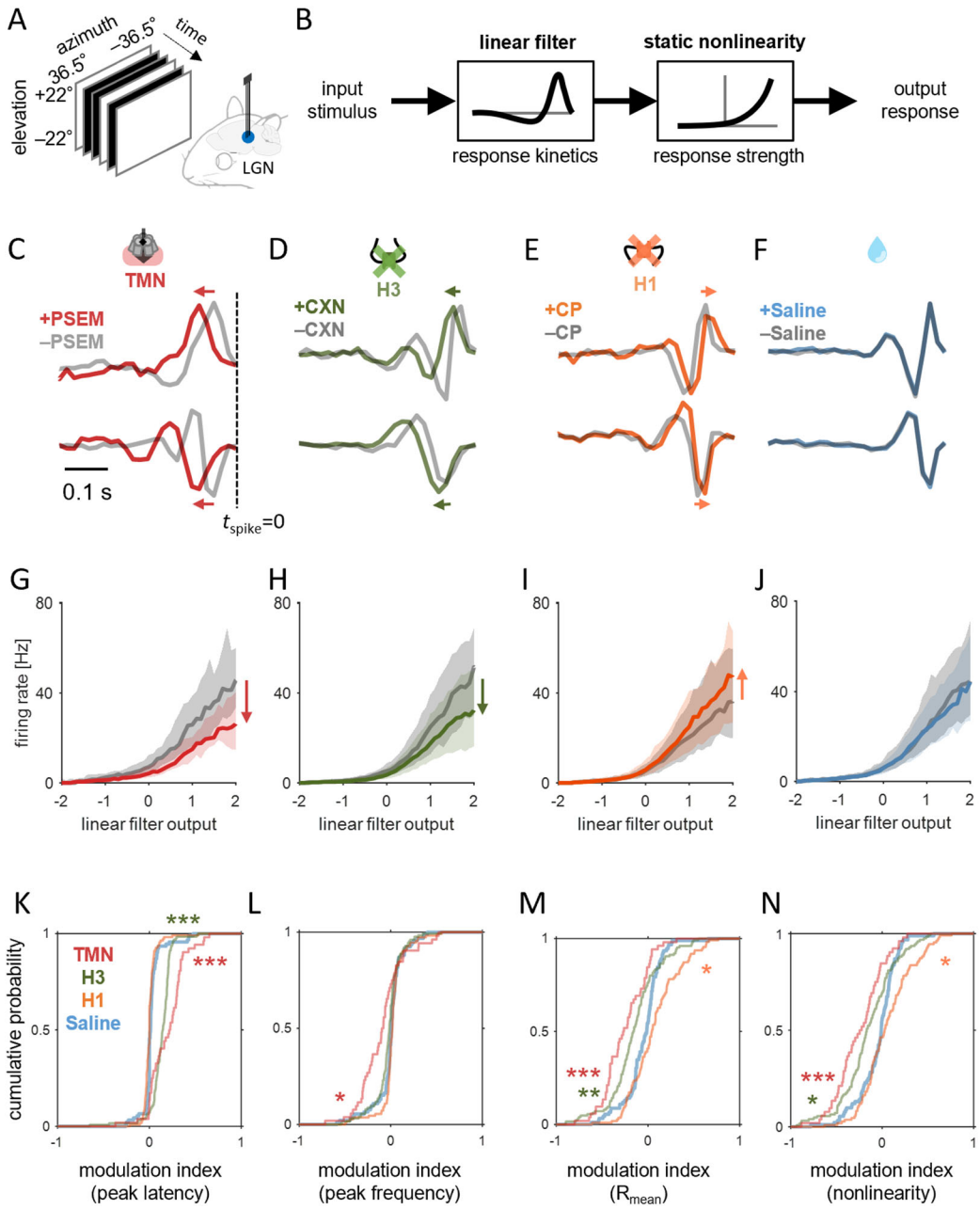

Figure 2: Histamine made the visual responses of LGN weaker and slower in awake head-fixed mice. *A,B*: Schematic diagram of LGN recordings (A) and linear-nonlinear cascade model (B). Reverse-correlation was used to estimate the linear filter and static nonlinearity that represent response kinetics and strength, respectively. *C*: Linear filters of two representative LGN cells before (gray) and after chemogenetic activation of HDC+ cells in TMN (red). We focused only on those data when the animal stayed stationary (<2 cm/s) to minimize the side effect of locomotion behavior (Supplementary Figure 3). *D-F*: Representative LGN linear filters before (gray) and after pharmacological treatment (D, 12 mg/kg ciproxifan, green; E, 5 mg/kg chlorphenamine, orange) or saline injection (F). *G-J*: Static nonlinearities averaged across LGN population before and after treatment in corresponding colors (G, chemogenetics, n=52 from 3 animals; H, ciproxifan, n=126 from 4 animals; I, chlorphenamine, n=110 from 3 animals; J, saline, n=92 from 3 animals): line, median; gray shade, 25 and 75 percentiles. *K-N*: Cumulative distributions of the modulation index before and after each treatment (in corresponding color): peak latency (K) and frequency (L) of the linear temporal filters, mean evoked firing rate during stimulation (M), and static nonlinearity (i.e., response gain; N): *, p<0.05; **, p<0.01; ***, p<0.001 from the post-hoc test against the saline control on the average group ranks (Kruskal-Wallis test).

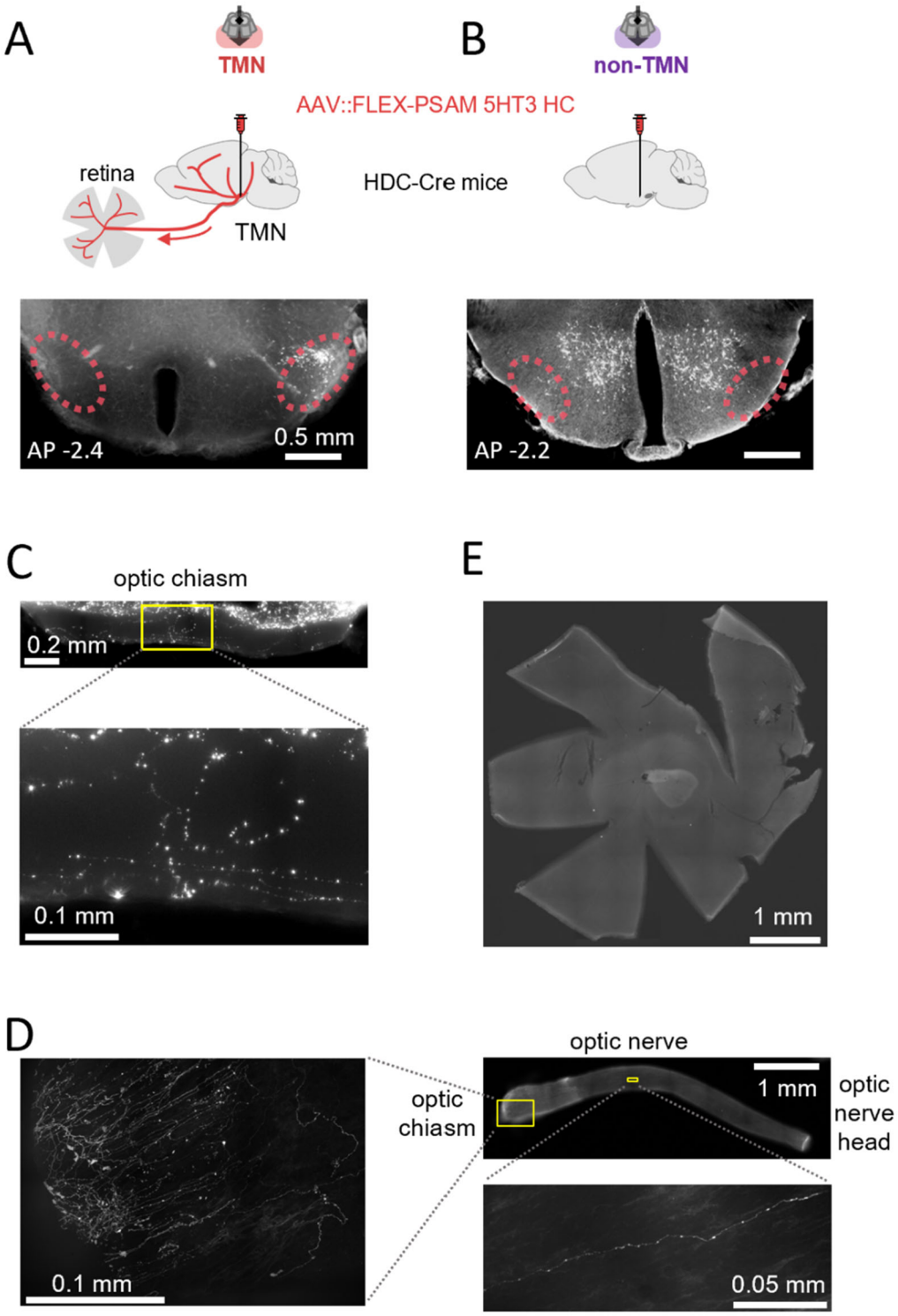

Supplementary Figure 2: Pharmacological and chemogenetic approaches to manipulate the central histaminergic system in the mouse brain. *A,B*: Viral delivery of PSAM 5HT3HC channel to HDC+ cells in the TMN (marked with dotted lines) of the posterior hypothalamus (A) or those in the anterior hypothalamus (B; control). *C-E*: Histological image examples of anterograde tracing of HDC+ cells in TMN. Labelled axons were found in the optic chiasm (C) or the optic nerve (D) after injecting rAAV9::CAG-FLEX-Synaptophysin-GFP or AAV2/1::CAG-FLEX-axon-GFP, respectively, in the TMN of HDC-Cre mice. However, no visible signal was detected in the isolated retinal tissue of all animals examined (n=9; see panel E for example).

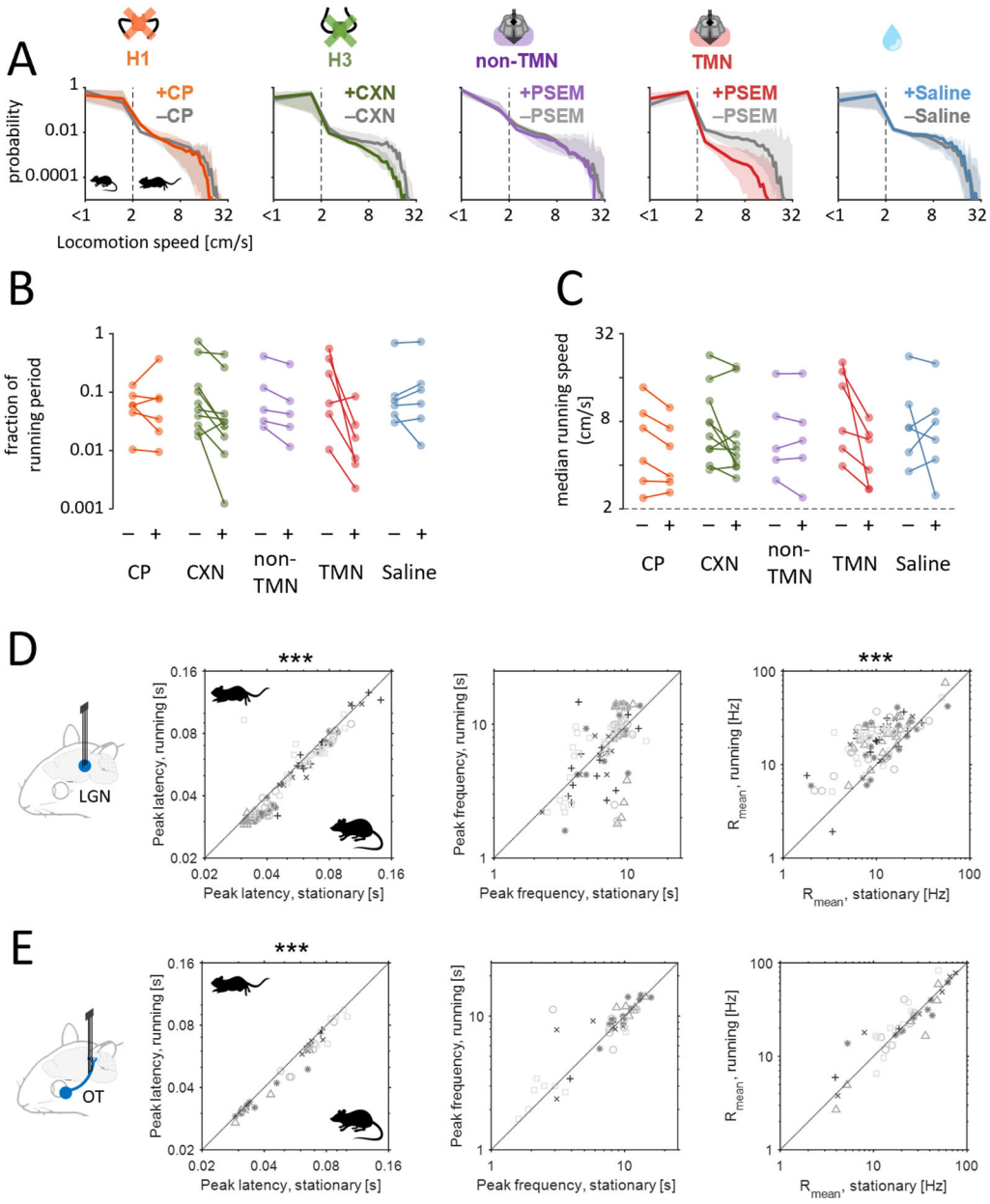

Supplementary Figure 3: Locomotion of an animal facilitates the visual responses of LGN and RGCs. *A*: probability distribution of an animal's locomotion speed during recordings before (gray) and after treatment: from left to right, chlorphenamine (CP, orange), ciproxifan (CXN, green), PSAM/PSEM for HDC+ cells in non-TMN (purple) or TMN (red), and saline (blue). *B*: the fraction of running period (>2cm/s) before and after each treatment. No significant change was observed (p=0.07, Kruskal-Wallis test). *C*: the median locomotion speed (during which animals moved at >2 cm/s) before and after each treatment. No significant change was observed (p=0.3). *D*: comparison of the LGN population response properties between stationary and running periods (n=104 from 5 animals with a running period ranging between 20% and 80%): from left to right, peak latency (50±19 ms versus 48±19 ms, median ± median absolute deviation; p<0.001, Wilcoxon signed-rank test), peak frequency (8.2±1.9 Hz versus 8.2±3.0 Hz; p=0.4), mean firing rate (11±6 Hz versus 20±8 Hz; p<0.001). *E*: corresponding data for RGCs (n=44 from 5 animals with a running period ranging between 20% and 80%): from left to right, peak latency (58±19 ms versus 49±18 ms; p<0.001), peak frequency (8.2±2.8 Hz versus 9.2±2.7 Hz; p=0.6), mean firing rate (24±22 Hz versus 23±22 Hz; p=0.5).

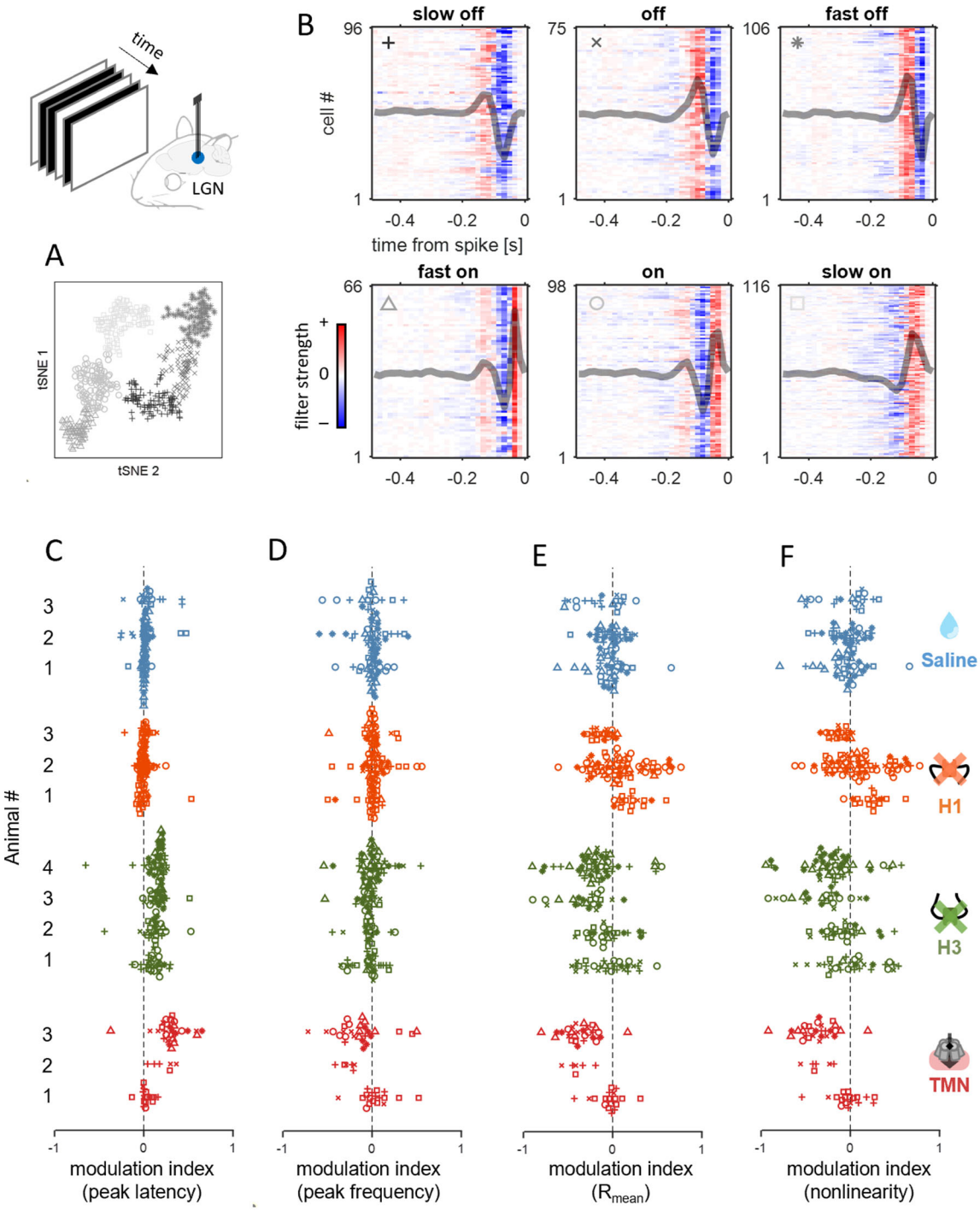

Supplementary Figure 4: Functional classification of LGN visual response types and batch effect analysis. *A*: t-SNE embedding of the STAs of LGN cells. Different markers and shadings are used for distinct response categories (shown in B). *B*: Each panel represents one of the six response categories: slow off, off, fast off, fast on, on, and slow on. In each panel, each row represents a cell's STA (color-coded with red and blue hue, indicating positive and negative filter values, respectively); and the overlaid gray line shows the average STAs in each response type. *C-F*: Modulation indices on LGN response characteristics across individual animals: from left to right, peak latency (C), peak frequency (D), mean evoked firing rate (E), and nonlinearity (F). The effects of histamine were largely consistent across animals.

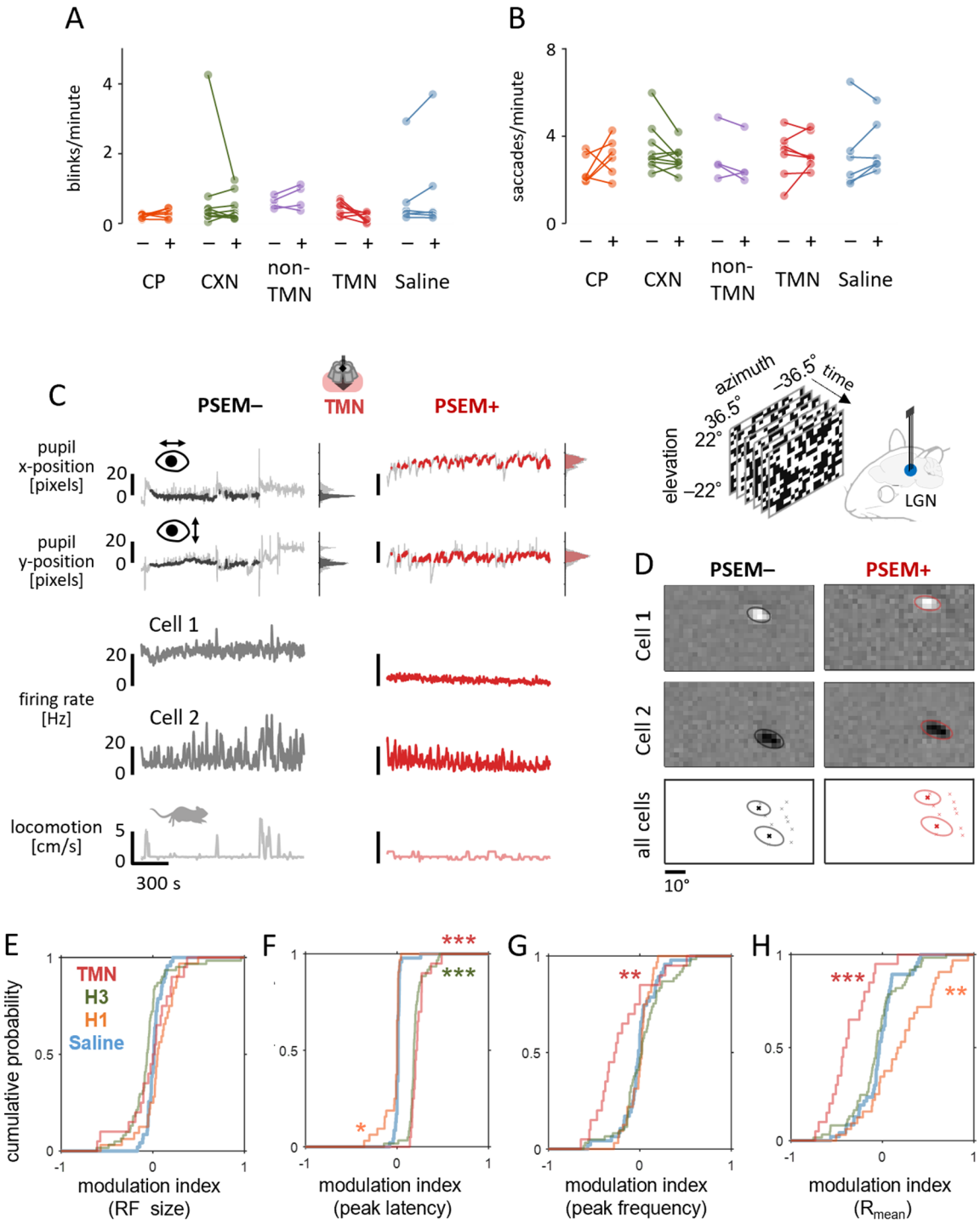

Supplementary Figure 5: Histamine did not affect LGN RF size. *A.B*: Blink (A) and saccade (B) frequencies before and after different treatments: from left to right, chlorphenamine (CP), ciproxifan (CPN), PSAM/PSEM for non-TMN HDC+ cells and TMN HDC+ cells, and saline. None of these changes were statistically significant: p=0.10, Kruskal-Wallis test on blink frequency changes; p=0.15, saccade frequency changes. *C*: Representative time series of the eye position (X- and Y-coordinates of the pupil center extracted from eye-tracking camera images) during white-noise "checkerboard" stimulation (black/red, centered and stable eye position used for reverse correlation; gray, non-centered or non-stable period excluded from the analysis; probability distribution shown on the right), before (left) and after (right) chemogenetic activation of TMN HDC+ cells. *D*: Estimated spatial filter (receptive field; RF) of two example LGN cells before (top) and after (bottom) chemogenetic activation of HDC+ cells in TMN. Note a shift of RF position of all recorded cells due to a shift of the animal's resting

eye position after the treatment (see panel C). *E-H*: Cumulative distribution of the modulation index of LGN cells before and after treatment (E, receptive field size; F, peak latency; G, peak frequency; H, mean evoked firing rate): orange, chlorphenamine, n=32 from 3 animals; green, ciproxifan, N=61 from 4 animals; red, PSAM/PSEM for HDC+ cells in TMN, N=20 cells from 3 animals. Post-hoc test against saline control (N=47 from 3 animals) after Kruskal-Wallis test: *, $p<0.05$; **, $p<0.01$; ***, $p<0.001$.

246 ## Histaminergic modulation starts from the mouse retina

247 Histaminergic neurons are localized solely in the hypothalamus, most densely in TMN, and
248 project their axons widely across the brain (Lin et al., 2023), including the mouse retina
249 (Gastinger et al., 1999; Repérant et al., 2007; Warwick et al., 2024). To test if the observed
250 histaminergic modulation of the visual processing in LGN originates in the retina, we next
251 performed in vivo optic tract (OT) recordings to monitor the retinal output responses in awake
252 head-fixed mice (Figure 3A,B; Boissonnet et al., 2023) before and after manipulating the
253 central histaminergic system (Figure 3 and Supplementary Figures 6-9).

254 Consistent with the results in LGN, chemogenetic activation of HDC+ neurons in TMN
255 led to reduced firing of retinal ganglion cells (RGCs; median, -9.8 Hz; IQR, 13.1 Hz; p=0.01;
256 n=26 from 4 animals) with lower response gain (median, -28%; IQR, 57 %; p=0.01); and slower
257 response kinetics with elongated linear temporal filters(Figure 3C,G; peak latency change,
258 median, 10 ms; IQR, 33 ms; p<0.001; peak frequency change, median, -17%; IQR, 34%,
259 p=0.003). We also found that the latencies of the peak responses to stimulus onset and offset
260 were both significantly longer, with a reduced peak firing (Supplementary Figure 6A,F). In
261 contrast, no change in these response parameters was observed when targeting HDC+
262 populations in the anterior hypothalamus outside TMN for the PSAM/PSEM activation (firing
263 rate change, median, 1.7 Hz, IQR, 16.5 Hz, p=0.6; gain change, median, 8%, IQR, 99%,
264 p=0.5; latency change, median 0 Hz, IQR, 12 Hz, p=0.6; frequency change, median -6%, IQR,
265 17%, p(U-test)=0.09; N=23 from 3 animals). Neither the onset nor the offset stimulus response
266 was affected (Supplementary Figure 6B,G). Anterograde tracing of HDC+ cells – via injection
267 of Cre-dependent AAVs encoding fluorescent marker proteins into the TMN of HDC-Cre
268 animals – showed labelled axons in the optic chiasm and/or the optic nerve (3 out of 9 animals;
269 Supplementary Figure 2C,D). Unlike previous reports (Gastinger et al., 1999; Repérant et al.,
270 2007; Warwick et al., 2024), however, we did not identify any labelled axons in the retinal
271 tissues (e.g., Supplementary Figure 2E), likely because these projections are sparse and
272 located far from the cell bodies, making the signals too weak. Nonetheless, our data

273 collectively support that the histaminergic modulation of the early visual system is mediated
274 by the centrifugal projections specifically from TMN (Figure 3G-J and Supplementary Figure
275 2).

276 The effects of the pharmacological treatments were overall similar between LGN and
277 RGCs, though certain differences existed. First, pharmacologically blocking the H3 receptors
278 with ciproxifan led to slower response kinetics in both LGN and RGCs (latency change, median,
279 10 ms; IQR, 14 ms; $p<0.001$; frequency change, median, -7%; IQR, 25%; $p=0.12$; N=36 from
280 4 animals), but the firing rates and the response gain remained largely unaffected in RGCs
281 (Figure 3D,H; firing rate change, median -0.1 Hz; IQR, 12.7 Hz; $p=0.3$; gain change, median,
282 -7%; IQR, 69%, $p=0.5$). This was also the case with the peak onset/offset stimulus responses
283 (Supplementary Figure 6C,H). Second, while chlorphenamine (H1 antagonist) drove faster
284 kinetics with marginally higher firing in both LGN and RGCs, the effects on the temporal filters
285 were primarily on the peak frequencies in LGN (Figure 2E) but on the peak latencies in RGCs
286 (Figure 3E; latency change, median, -5 ms; IQR, 8 ms; $p=0.006$; frequency change, median,
287 +4 Hz; IQR, 25 Hz; $p=0.6$; firing rate change, median, +2 Hz, IQR, 11 Hz; $p=0.09$; gain change,
288 median, 4%, IQR, 90%, $p=0.3$; N=33 RGCs from 3 animals). Likewise, a shorter peak latency
289 was observed in the onset/offset stimulus responses of RGCs (Supplementary Figure 6D,I).
290 Finally, RGC receptive fields did not show significant changes in size, either (Supplementary
291 Figure 8).

292 Although diverse effects of histamine across retinal cell types have been reported in
293 previous ex vivo studies (Gastinger et al 2004; Yu et al., 2009, 2011; Akimov et al., 2010; Vila
294 et al., 2012; Horio et al., 2018; Warwick et al., 2024), the histaminergic effects observed in this
295 study were rather uniform across RGC or LGN populations. First, the effects on the peak
296 responses to the contrast-inverting stimuli did not significantly differ between the stimulus
297 onset and offset (Figure 1 and Supplementary Figure 2). Second, the effects on the temporal
298 filter and nonlinearity were not substantially different among the six functional groups that we
299 identified for RGCs and LGN cells, respectively (Supplementary Figures 4 and 7). Our

300 datasets are, however, not large enough to identify all the ~40 physiological cell-types reported
301 thus far (Baden et al., 2016; Rosón et al., 2019); and we could not target a specific cell-type
302 or tailor visual stimuli for each cell during recordings due to technical limitations. Lastly, we
303 identified direction-selective (DS) and orientation-selective (OS) cells using the responses to
304 moving grating stimuli in eight different directions (see Methods for details), but we found no
305 differences in the DS or OS index values – defined by the normalized population vector length
306 – before and after each treatment (Supplementary Figure 9).

307 Taken all together, our data indicate that 1) the mouse early visual processing is
308 subject to histaminergic modulation controlled by TMN, starting from the retina; 2) histamine
309 generally suppresses the firing and slows the response kinetics; and 3) response latency and
310 frequency tuning are likely modulated by different mechanisms.

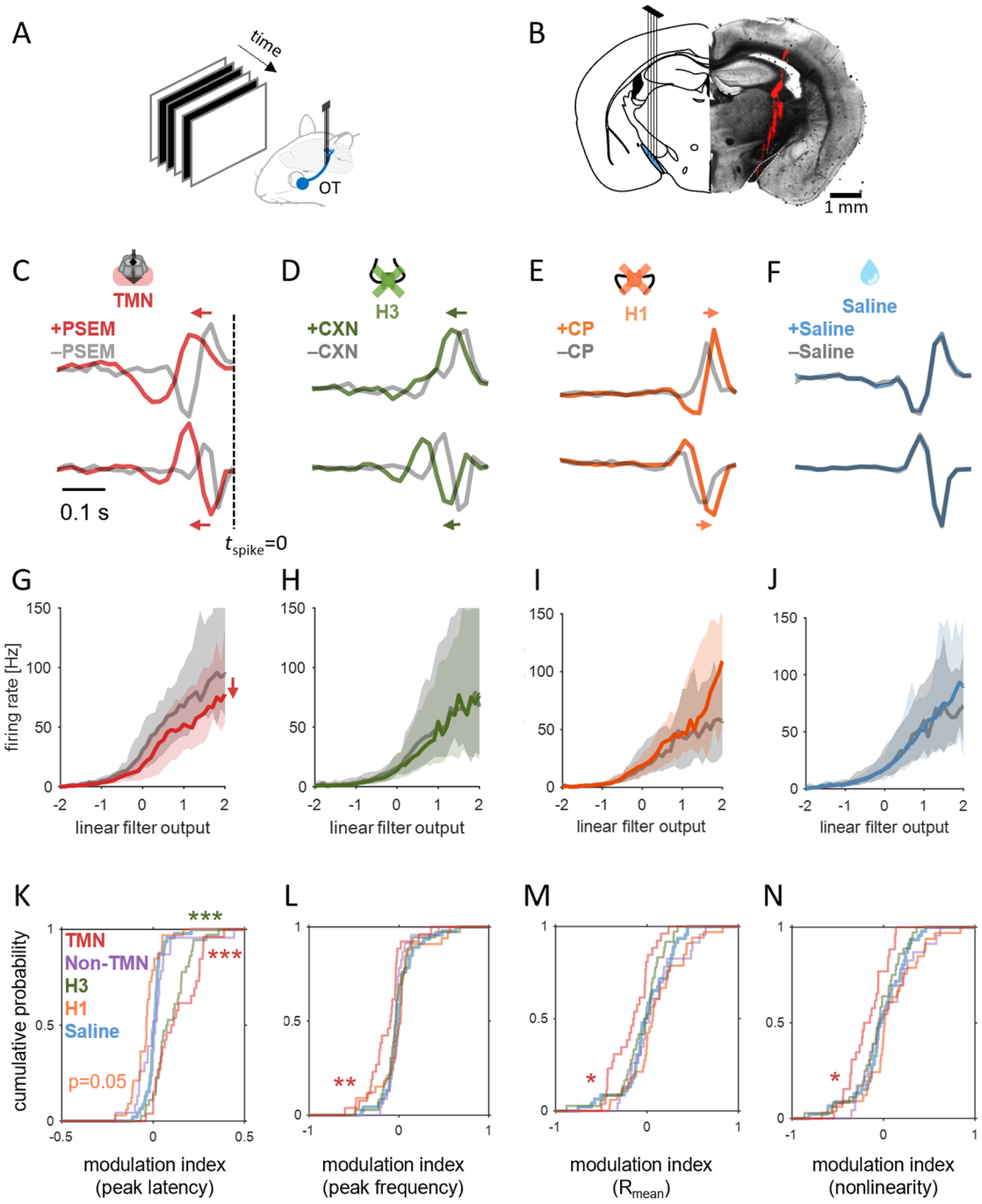

Figure 3: histamine primarily affected the visual response kinetics of RGCs. *A,B*: Schematic diagram of in vivo optic tract (OT) recordings (A) and a representative histological image showing the electrode location (B; DiI stain, red). *C-F*: Linear filters of two representative RGCs before (gray) and after chemogenetic (A, red) or pharmacological treatment (B, 12mg/kg ciproxifan, green; C, 5 mg/kg chlorphenamine, orange; D, saline, blue). *G-J*: Static nonlinearities averaged across RGC population before and after treatment in corresponding colors (G, chemogenetics, n=26 cells from 4 animals; H, ciproxifan, n=36 from 4 animals; I, chlorphenamine, n=33 from 3 animals; J, saline, n=46 cells): line, median; gray shade, 25 and 75 percentiles. *K-N*: cumulative distributions of the modulation index before and after each treatment (in corresponding color; n=23 from 3 animals for chemogenetic treatment of non-TMN HDC+ cells): peak latency (K) and frequency (L) of the linear temporal filters, mean evoked firing rate during stimulation (M), and static nonlinearity gain function (N); *, p<0.05; **, p<0.01; ***, p<0.001 from the post-hoc test against the saline control condition in the average group ranks (Kruskal-Wallis test).

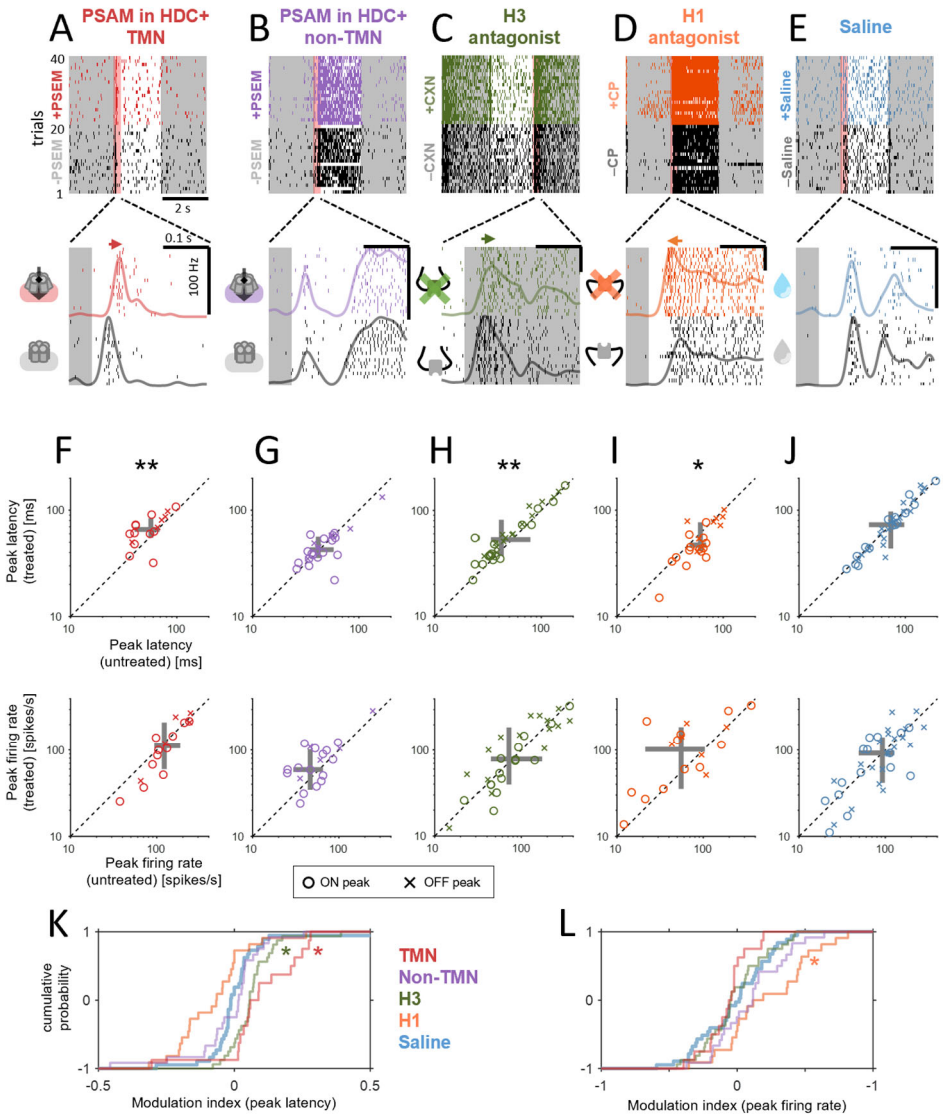

Supplementary Figure 6: histamine primarily modulated the visual response kinetics of RGCs. *A-E*: Visual responses of a representative RGC to full-field contrast-inverting stimuli (2 s intervals) before and after chemogenetic (A, HDC+ cells in TMN; B, HDC+ cells in non-TMN) or pharmacological treatment (C, ciproxifan; D, chlorphenamine; E, saline); top, spike raster across trials; bottom, zoom-in of the spike raster around stimulus onset or offset (-50 ms to 250 ms, red shade on top) and peri-stimulus time histogram. *F-J*: pairwise comparison of the RGC population responses before and after treatment (top, peak latency; bottom, peak firing rate): *, p<0.05; **, p<0.01, Wilcoxon signed-rank test with Bonferroni correction. F, PSAM/PSEM for TMN HDC+ cells: 57±15 ms versus 66±17 ms peak latency, p=0.005; 122±54 Hz versus 112±66 Hz peak frequency, p=0.08; median ± median absolute deviation, n=16 RGCs from 4 animals. G, PSAM/PSEM for non-TMN HDC+ cells: 42±17 versus 43±14 ms peak latency, p=0.3; 46±30 Hz versus 59±40 Hz peak frequency, p=0.3; n=24 RGCs from 3 animals. H, ciproxifan: 42±31 ms versus 53±31 ms peak latency, p=0.002; 72±80 Hz versus 78±78 Hz peak frequency, p=0.3; n=32 RGCs from 4 animals. I, chlorphenamine: 61±16 ms versus 47±18 ms peak latency, p=0.026; 55±60 Hz versus 102±88 Hz peak frequency, p=0.05; n=22 RGCs from 3 animals. J, saline: 73±30 ms versus 73±31 ms peak latency, p=0.5; 92±50 Hz versus 92±56 Hz peak frequency, p=1; n=37 RGCs from 3 animals. *K,L*: cumulative distributions of the modulation index before and after each treatment (in corresponding colors): K, peak latencies; L, peak firing rate; *, p<0.05 from the post-hoc test against the saline (control) condition on the average group ranks (Kruskal-Wallis test).

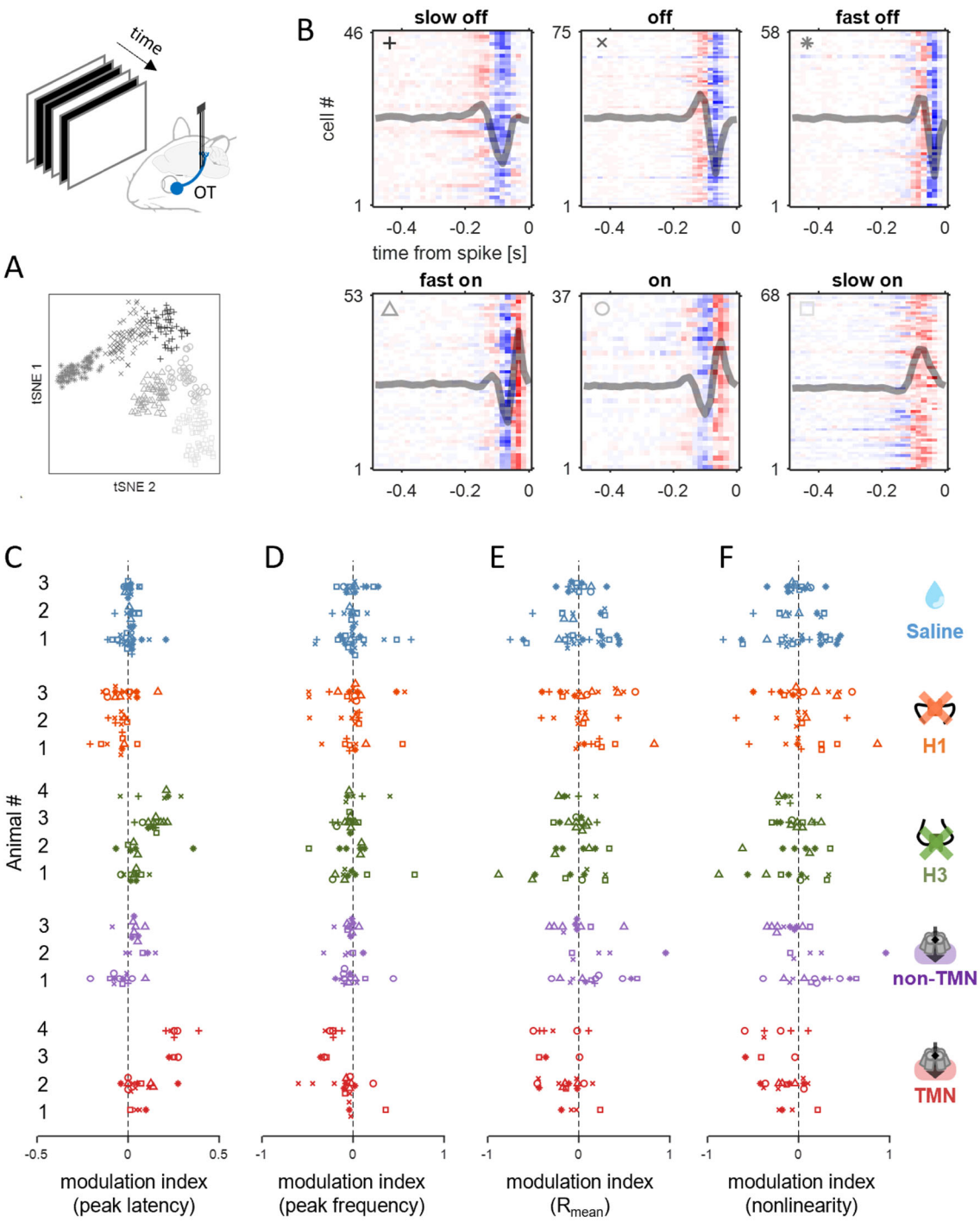

Supplementary Figure 7: Functional classification of RGC visual response types and batch effect analysis. *A*: t-SNE embedding of the RGC STAs. Different markers and shadings are used for distinct response categories (shown in B). *B*: Each panel represents one of the six response categories: slow off, off, fast off, fast on, on, and slow on. In each panel, each row represents a cell's STA (color-coded with red and blue hue, indicating positive and negative filter values, respectively); and the overlaid gray line shows the average STAs in each response type. *C-F*: modulation indices on RGC response characteristics across animals: from left to right, peak latency (C), peak frequency (D), mean firing rate (E), and nonlinearity (F). The effects of histamine were generally consistent across animals, and no substantial batch effect was observed.

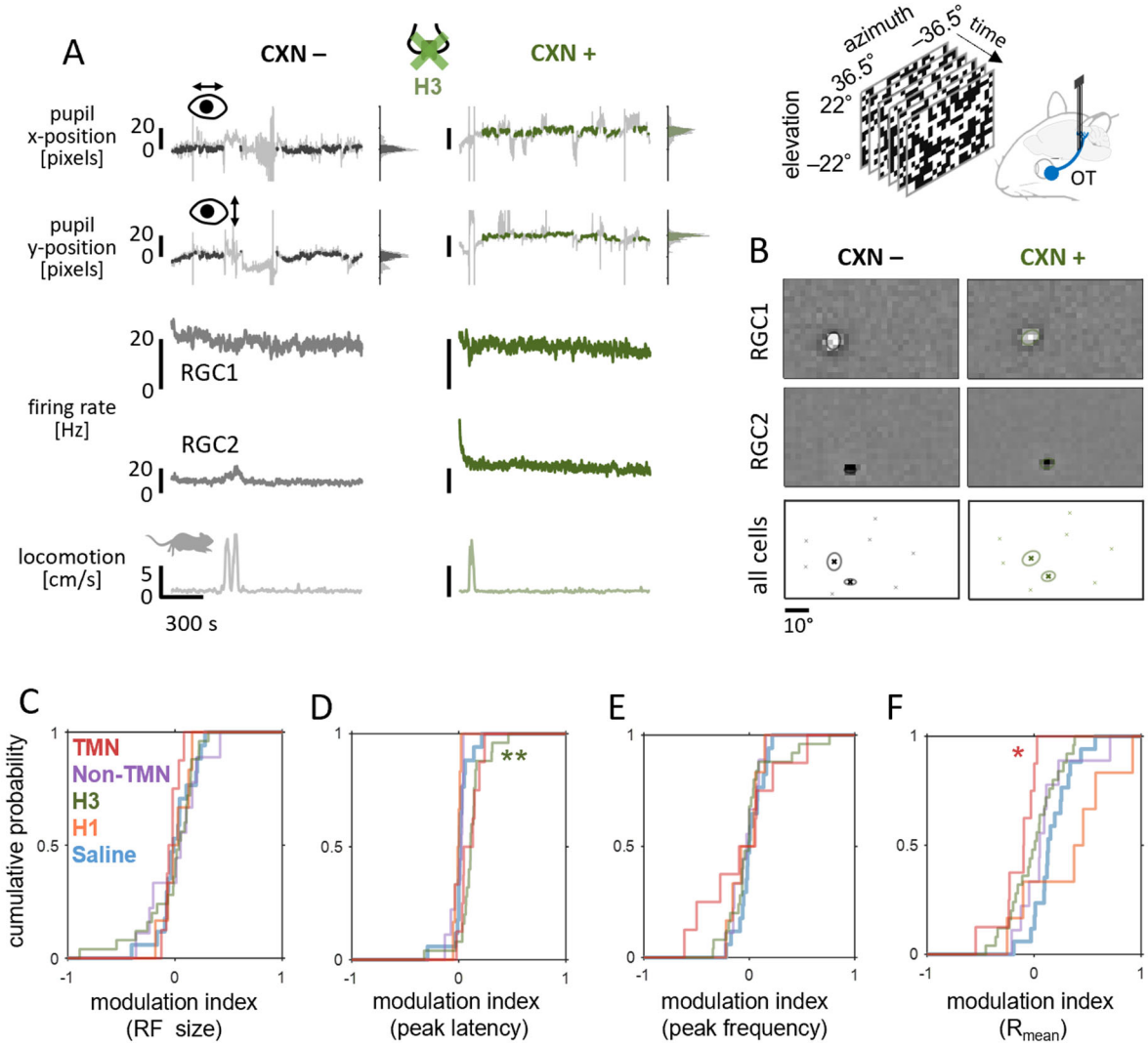

Supplementary Figure 8: Histamine did not affect RGC RF size. *A*: Representative time series of the eye position (X- and Y-coordinate of the pupil center extracted from eye-tracking camera images) during white-noise "checkerboard" stimulus presentation (black/green, centered and stable eye position used for reverse correlation analysis; gray, non-centered or non-stable period excluded from the analysis; probability distribution shown on the right), along with those of firing rate dynamics of two example RGCs and locomotion (from top to bottom), before (left) and after (right) ciproxifan administration. *B*: Estimated spatial filter (receptive field) of the two example RGCs (top and middle) before (left) and after (right) ciproxifan administration. Note a shift of RF position of all recorded cells due to a shift of resting eye position after the treatment (see panel A). *C-F*: cumulative distribution of the modulation index of RGCs before and after treatment (E, receptive field size; F, peak latency; G, peak frequency, H, mean firing rate): orange, chlorphenamine, n=6 cells from 3 animals; green, ciproxifan, n=25 cells from 4 animals; purple, PSAM/PSEM for HDC+ cells in non-TMN, n=9 cells from 3 animals; red, PSAM/PSEM for HDC+ cells in TMN, n=8 cells from 4 animals. Post-hoc test against saline control (N=17 from 3 animals) after Kruskal-Wallis test: *, $p<0.05$; **, $p<0.01$.

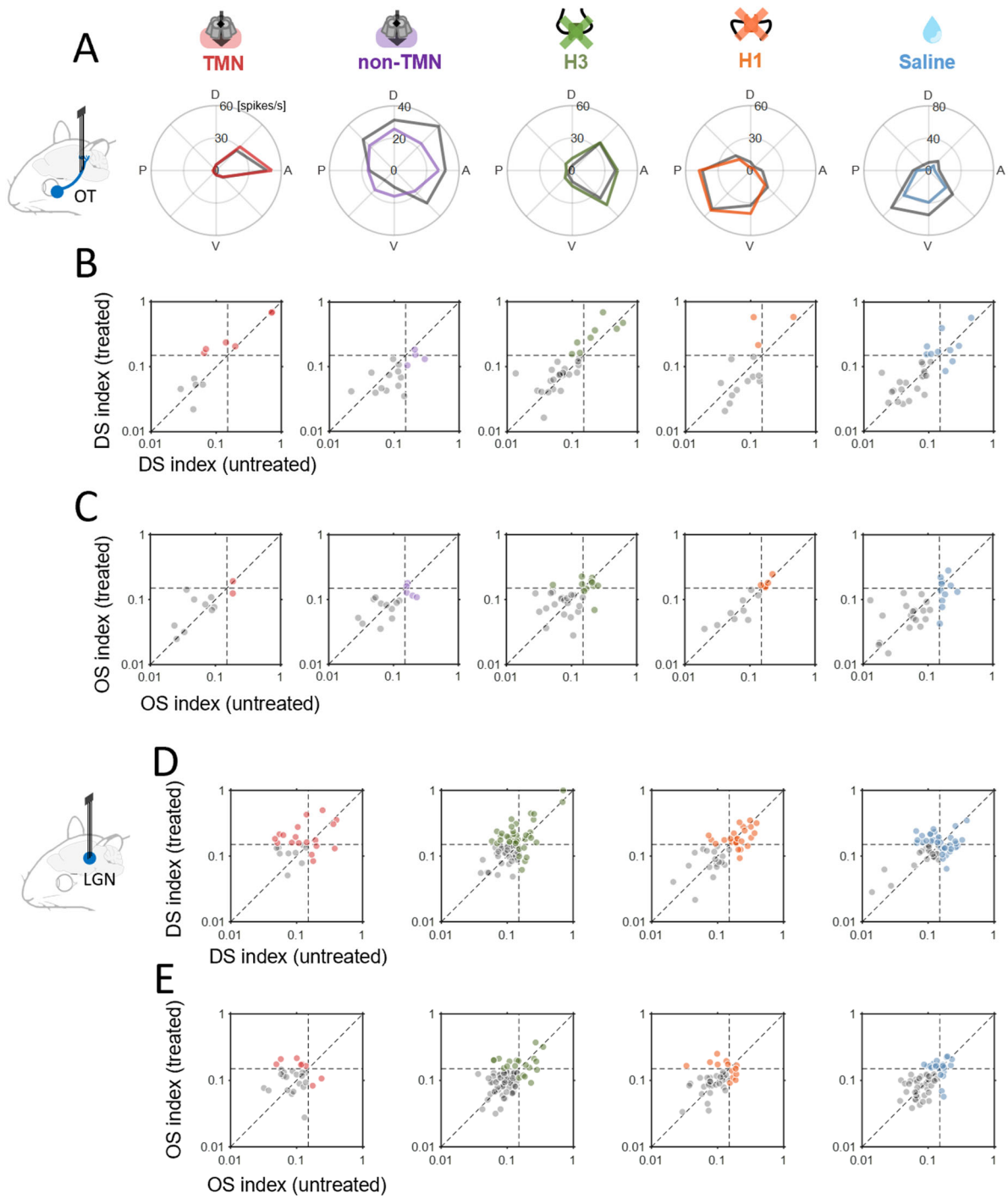

Supplementary Figure 9: Histamine did not affect direction- or orientation-selectivity of RGCs or LGN cells. *A*: the average firing rate of a representative direction-selective (DS) RGC in response to moving gratings in eight different directions before (gray) and after treatment (color-coded): from left to right, PSAM/PSEM for TMN HDC+ cells (red) or non-TMN cells (purple), ciproxifan (green), chlorphenamine (orange), and saline (blue). *B*: DS indices of RGC populations before and after treatment. Those with DS index > 0.15 in either condition were highlighted in the corresponding color (from left to right, n=11, 16, 31, 14, and 30 RGCs, respectively). No significant change was observed in the DS index values: p>0.2 in all cases (Wilcoxon signed-rank test). *C*: Corresponding data for the OS indices of RGCs. No significant change was observed (p>0.7 in all cases). *D,E*: Corresponding population data for the DS and OS indices of LGN cells (from left to right, n=42, 76, 27, 58 LGN cells; p>0.06 and 0.3 in all cases, respectively).

Pupil dynamics and locomotion are irrelevant to histaminergic modulation of the early visual processing in mice

Histamine is a potent neuromodulator implicated in various brain functions and behaviors, such as sleep-wake cycles and arousal (Haas and Panula, 2003; Thakkar, 2011). Thus, it is possible that the observed histaminergic effects on the visual response properties in the mouse early visual system are a result of correlated behavioral modulation. For example, a larger pupil size leads to stronger responses because more photons reach the retina (Boissonnet et al., 2023). To address this issue, we examined the relationship between the histaminergic effects on the RGC/LGN visual responses and simultaneously monitored behavioral measures (Figure 4 and Supplementary Figure 10).

We first assessed the effects of the pupil size on the RGC/LGN visual responses. In particular, we performed the reverse correlation analysis using subsampled data with a constricted or dilated pupil for each recording (below 33 or above 66 percentiles of the pupil size, respectively; e.g., Figure 4A-C). Under the control condition, we found that the larger the pupil size, the faster the response kinetics for both RGCs (Figure 4D,E) and LGN cells (Supplementary Figure 10A,B). We also found that the LGN responses were generally stronger with a dilated pupil than with a constricted pupil (Supplementary Figure 10C). In contrast, variations in the mean evoked firing rate of RGCs between constricted and dilated pupil periods were not uniform across the population, but dependent on their response polarity ($R=0.20$, $p=0.015$, Pearson's correlation with the temporal filter ON-OFF polarity index, defined by the difference between the peak and valley, normalized by the sum of the two; $n=152$ RGCs from 16 animals).

How does this pupil size effect interrelate with the histaminergic effect? As reported before (Fang et al., 1998), chlorphenamine (H1 antagonist) led to a substantial increase in the baseline pupil size due to its anticholinergic action (Figure 4K; 67±34%, mean ± standard deviation of the median pupil size, $n=6$ animals). We compared the RGC kinetics after blocking

413 H1 with a constricted pupil (hence relatively slower) to those before the treatment with a dilated
414 pupil (hence relatively faster), and found no significant difference (Figure 4M). Thus, we cannot
415 exclude a possible contribution of the baseline pupil dilation to the response facilitation effect
416 of chlorphenamine. In contrast, chemogenetic activation of TMN HDC+ cells resulted in a
417 slight increase in the baseline pupil size (2±23%, n=6 animals), while ciproxifan (H3
418 antagonist) treatment led to a slight decrease (Figure 4K; -7±18%, n=8 animals), though they
419 both resulted in slower RGC/LGN response dynamics (Figure 3 and Supplementary Figure 6).
420 Such discrepancies are likely due to side effects of the manipulations beyond histamine: e.g.,
421 ciproxifan has modest affinity to adrenergic receptors (Esbenshade et al., 2003) and inhibits
422 monoamine oxidase A and B (Hagenow et al., 2017), while some HDC+ cells co-release
423 histamine and GABA (Yu et al., 2015). Here we found that the response kinetics of RGC/LGN
424 after these manipulations with a dilated pupil (hence relatively faster) were nevertheless
425 slower than those under the control condition with a constricted pupil (hence relatively slower;
426 Figure 4L). Therefore, the resulting slow response kinetics after up-regulating histamine
427 cannot be attributable to the pupil size effects.

428 We next analyzed the effect of pupil dynamics. In general, changes in pupil size occur
429 much more slowly than the response dynamics of the early visual system: e.g., pupillary light
430 reflex has a latency of hundreds of milliseconds and a time-constant of about a second
431 (Grozdanic et al., 2009; Liu et al., 2017). Nevertheless, when the pupil is dilating, presented
432 stimuli on the screen should appear brighter on the retina than intended, allowing RGCs to
433 respond to physically darker stimuli and thereby biasing the response polarity balance.
434 Conversely, one would expect the opposite effect when the pupil is constricting. We indeed
435 identified the corresponding changes in the ON/OFF balance of both RGC and LGN responses
436 (Figure 4G and Supplementary Figure 10D), using the temporal filter ON-OFF polarity index.
437 An increase of the mean evoked firing rate was also observed in LGN, but not in RGCs, during
438 pupil dilation (Figure 4J and Supplementary Figure 10G). However, no change in the response
439 kinetics were observed in both RGCs and LGN between dilating and constricting pupil periods

440 (Figure 4H,I and Supplementary Figure 10E,F). The frequencies of saccades or eye blinks did
441 not change, either, after the pharmacological or chemogenetic treatments (Supplementary
442 Figure 5A,B). We thus conclude that the pupil dynamics should have little to do with the
443 observed histaminergic effects on the RGC/LGN visual responses.

444 Locomotion has been reported to profoundly affect information processing throughout
445 the mouse visual system (Neil and Stryker, 2010; Erisken et al., 2014; Dipoppa et al., 2018;
446 Savier et al., 2019; Schröder et al., 2020). When we compared the temporal filter
447 characteristics during running and stationary periods (at a threshold of 2 cm/s), we indeed
448 found that locomotion facilitated visual responses of RGCs and LGN cells (Supplementary
449 Figure 3D,E). Importantly, we excluded these running periods from the analysis of the
450 histaminergic effects described above. Furthermore, the mice remained stationary most of the
451 time under the head-fixed condition (Supplementary Figure 3A), and neither the chemogenetic
452 nor the pharmacological treatments resulted in a significant change in either the fraction of
453 time spent running (Supplementary Figure 3B) or the median running speed (Supplementary
454 Figure 3C). Thus, locomotion and its effects on RGC/LGN responses are irrelevant to the
455 observed histaminergic modulation, and likely involve different mechanisms.

456 Taken together, neither pupil dynamics nor locomotion behavior was causally linked
457 with the histaminergic modulation of the mouse early visual system. We conclude that the
458 central histaminergic system modulates the mouse vision, effectively leading to slower and
459 weaker responses.

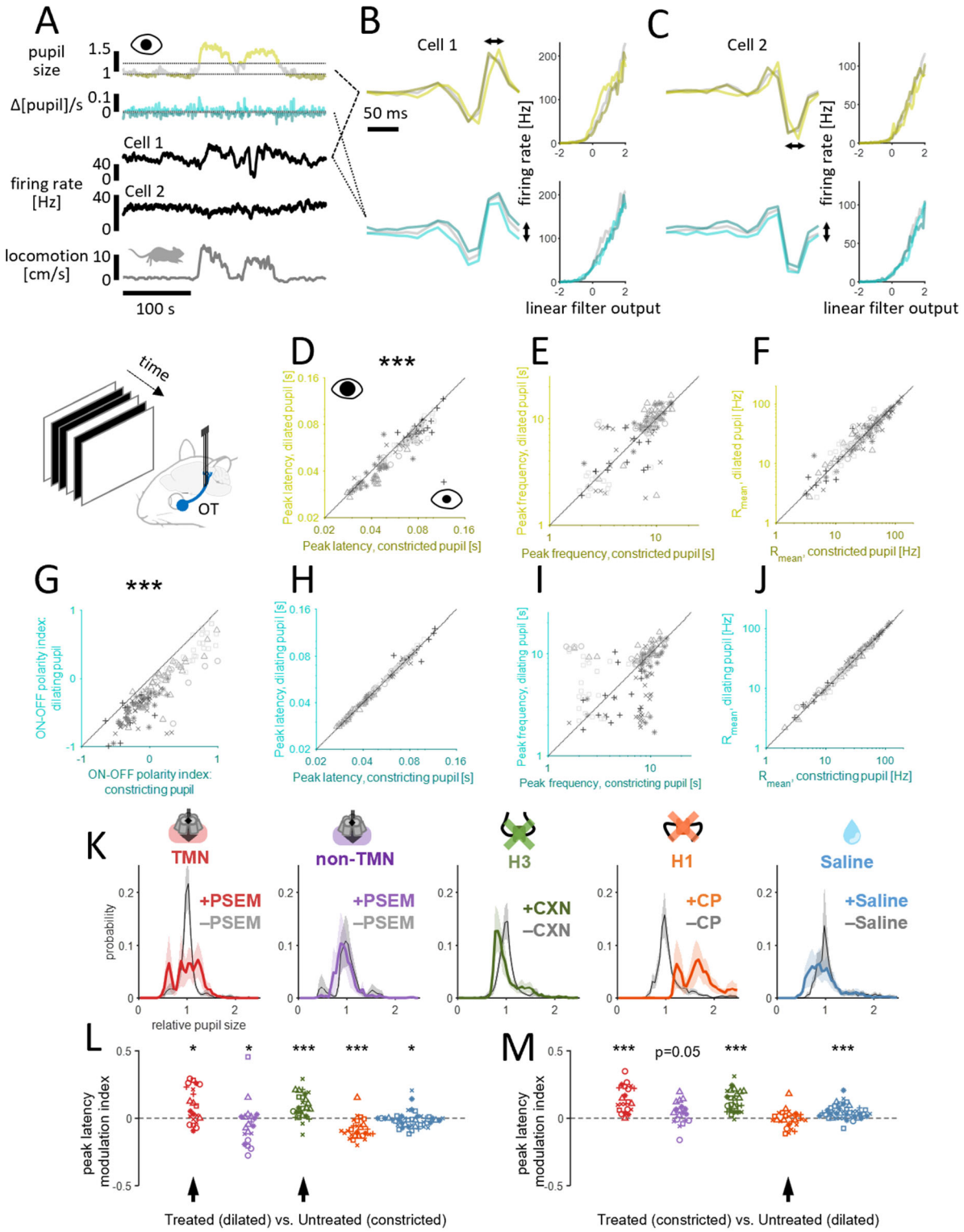

Figure 4: histaminergic modulation of pupil dynamics was not causally linked with that of RGC/LGN visual responses. *A*: Representative time series of the pupil size (light yellow, top 33 percentile; dark yellow, bottom 33 percentile) and its time derivative (light blue, positive; dark blue, negative) during randomly flickering full-field stimulus presentation, along with those of the firing rate dynamics of two example RGCs and locomotion (from top to bottom). *B*: Estimated linear filter and nonlinearity for a representative RGC (B, cell 1) using constricted or dilated pupil periods (top) or using constricting or dilating pupil periods (bottom). Note a temporal shift of the linear filter in the former case, while a shift in the filter strength in the latter. *C*: corresponding data for another RGC (cell 2). *D-F*: comparison of the RGC population

response properties between constricted and dilated pupil periods (n=152 RGCs from 16 animals): D, peak latency, 65±19 ms versus 60±17 ms, median ± median absolute deviation, p<0.001, Wilcoxon signed-rank test; E, peak frequency, 8.2±2.6 Hz versus 8.2±2.7 Hz, p=0.6; F, mean firing rate, 26±19 Hz versus 28±18 Hz, p=0.6. *G-J*: comparison of the RGC population response properties between constricting and dilating pupil periods: G, ON-OFF polarity index of the temporal filters, -0.02±0.33 versus -0.25±0.33, p<0.001; H, peak latency, 62±18 ms versus 63±18 ms, p=0.9; I, peak frequency, 8.3±2.8 Hz versus 8.3±3.0 Hz, p=0.9; J, mean firing rate, 26±18 Hz versus 28±19 Hz, p=0.7. *K*: probability distributions of relative pupil size before and after treatment: from left to right, PSAM/PSEM for TMN HDC+ cells (red) or non-TMN cells (purple), ciproxifan (green), chlorphenamine (orange), and saline (blue). *L*: comparison of peak latencies before treatment with constricted pupil versus after treatment with dilated pupil. Histamine nevertheless significantly slowed the RGC population responses (arrow heads): *, p<0.05; **, p<0.01; ***, p<0.001, Wilcoxon signed rank test. *M*: comparison of peak latencies before treatment with dilated pupil versus after treatment with constricted pupil. Effects of H1 blocker could not be distinguished from those of pupil dilation (arrow head, p=0.5).

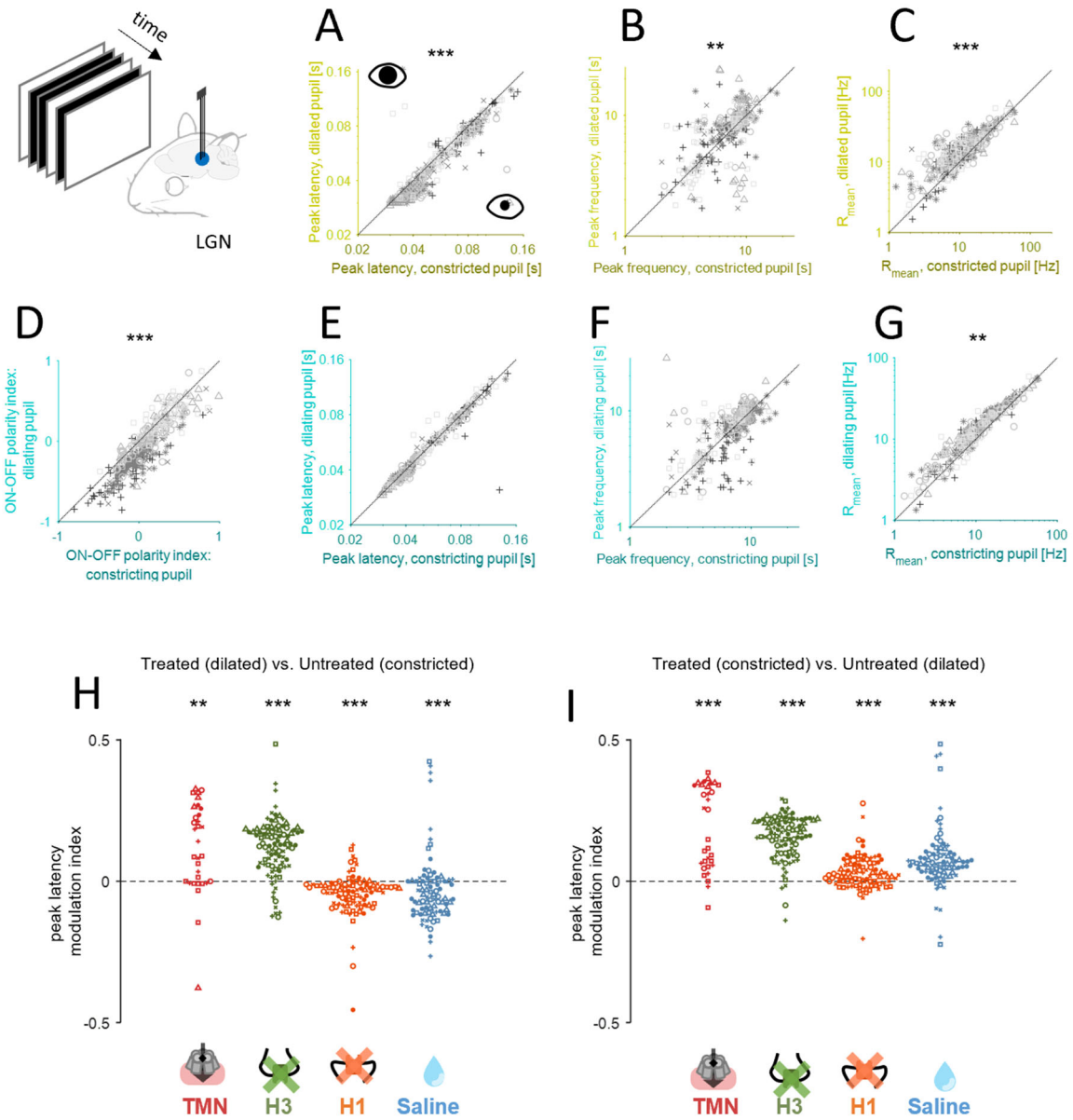

Supplementary Figure 10: Histaminergic effects on pupil dynamics are irrelevant to those on LGN visual responses. *A-C*: comparison of the LGN population response properties between constricted and dilated pupil periods (n=350 RGCs from 13 animals): A, peak latency, 51±20 ms versus 48±19 ms, median ± median absolute deviation, p<0.001, Wilcoxon signed-rank test; B, peak frequency, 7.9±2.1 Hz versus 8.1±2.4 Hz, p=0.004; E, mean firing rate, 11±7 versus 15±7 Hz, p<0.001. *D-G*: comparison of the LGN population response properties between constricting and dilating pupil periods: D, ON-OFF polarity index of the temporal filters, 0.07±0.22 versus -0.06±0.27, p<0.001; E, peak latency, 49±19 ms versus 49±19 ms, p=0.8; F, peak frequency, 7.9±2.0 Hz versus 8.1±2.1 Hz, p=0.3; G, mean firing rate, 11±7 Hz versus 14±7 Hz, p=0.004. H: comparison of peak latencies before treatment with constricted pupil versus after treatment with dilated pupil: from left to right, PSAM/PSEM for TMN HDC+ cells (red), ciproxifan (green), chlorphenamine (orange), and saline (blue): **, p<0.01; ***, p<0.001, Wilcoxon signed rank test. *I*: comparison of peak latencies before treatment with dilated pupil versus after treatment with constricted pupil.

Response gain modulation is more strongly correlated with peak latency modulation than with peak frequency modulation

What are the mechanisms underlying the histaminergic modulation of the early visual processing? To address this question, we next took a computational approach to examine the relationship between different aspects of the visual response properties that we identified to be affected by histamine (Figure 5). In particular, we simulated the activity of an integrate-and-fire neuron with Poisson spiking and refractoriness in response to white-noise input stimuli (Figure 5A), and processed the output spike trains in the framework of the linear-nonlinear cascade model to characterize the simulated response properties in the same way as the experimental data (Figure 2B). Here we varied two model parameters, gain and resting baseline, to examine the effects of their changes on the following four aspects of the simulated responses: spike counts, the peak latency and frequency of the estimated linear temporal filter, and the slope of the estimated static nonlinearity (expressed as half-wave rectification). The rest model parameters were fixed in all simulations, including the underlying linear filter given by a trigonometric function with logarithmic scale in time, and the refractory period filter given by an exponential function. The spike threshold was drawn from a random uniform distribution ranging from 0 to 1 for each time point to approximate the Poisson spiking properties.

When the model neuron had a higher gain or higher resting baseline, subthreshold signal reached the spike threshold faster and more frequently; hence, total spike counts became higher (Figure 5B) and the peak latency of the estimated linear temporal filter appeared shorter (Figure 5C). In contrast, the apparent peak frequency of the simulated responses was dependent more strongly on the resting baseline than on the gain (Figure 5D). These changes in the estimated linear temporal filter properties were consistent with the experimental observation, where the magnitude of the response gain modulation by histaminergic perturbation was significantly correlated with that of the peak latency modulation

527 (Figure 5F,H), but much less with that of the peak frequency modulation (Figure 5G,I). This
528 agreement between the observed and simulated data indicates that, despite the simplicity, our
529 model captures aspects of neuronal response modulation to a first approximation.

530 The model analysis supports that the histaminergic effects on RGCs should involve at
531 least gain and baseline modulations. First, the H1 receptors likely mediate the gain modulation
532 in RGCs, given that chlorphenamine (H1 antagonist) led to changes in the peak latency but
533 not the peak frequency, along with changes in the estimated static nonlinearity largely by
534 scaling (Figure 3). Second, the peak frequency was modulated as well as the peak latency of
535 RGCs upon chemogenetic activation of HDC+ neurons in TMN, accompanied by a shift of the
536 estimated static nonlinearity. This implies changes in the baseline resting potential of the cells.
537 Blocking the H3 receptors, however, led to changes in the RGC response kinetics without
538 much affecting the mean firing rates. Furthermore, the net effects of histamine perturbations
539 on LGN responses were more diverse (Figures 1 and 2) and not fully explainable by the simple
540 model (Figure 5). Thus, we expect that mechanisms besides gain and baseline modulations
541 are also involved, such as neural circuit effects through retinal amacrine cells for example
542 (Horio et al., 2018).

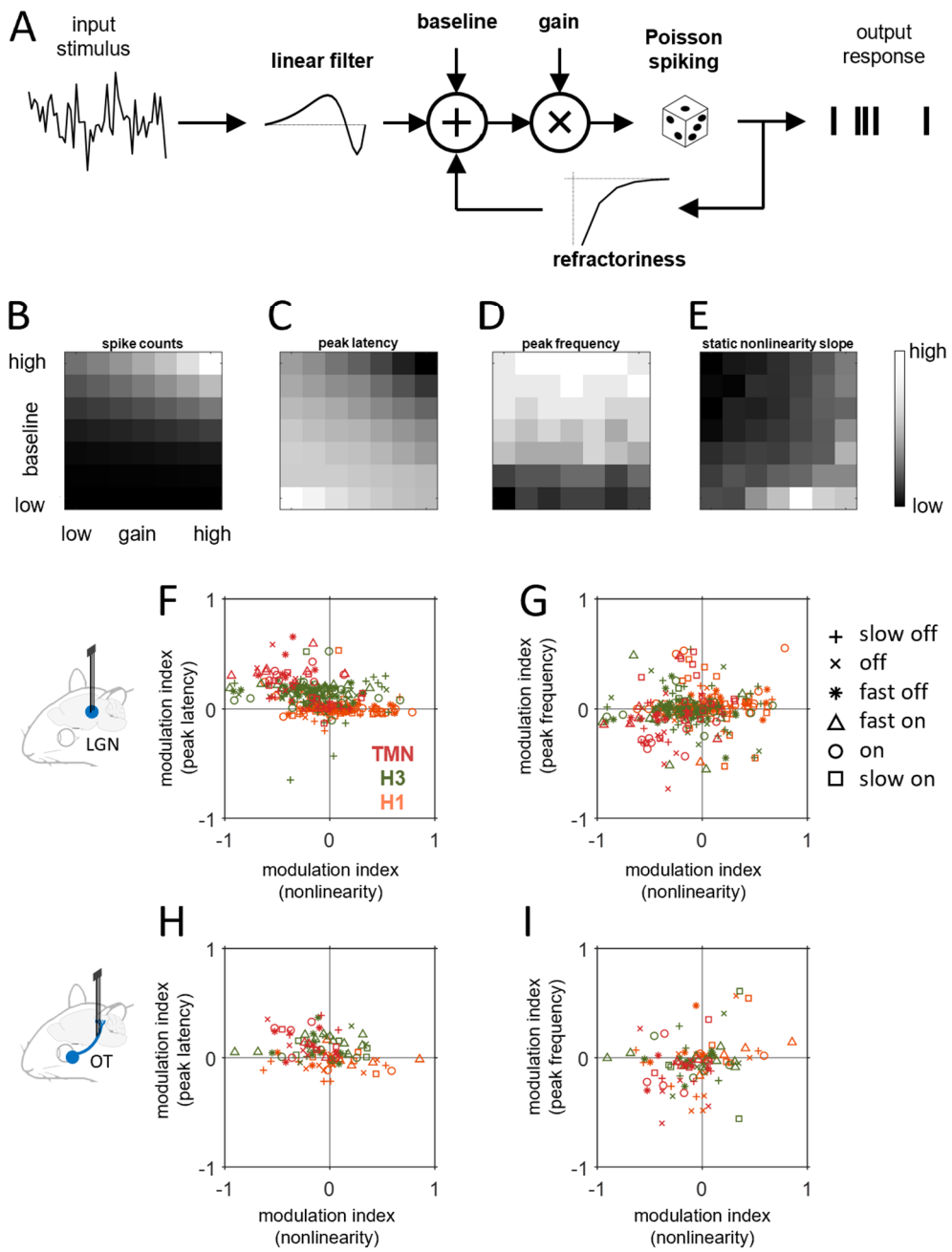

Figure 5: Gain modulation accompanies the peak latency modulation but not the peak frequency modulation via histaminergic effects. *A-E*: Using a computational model outlined in A, here we examined the consequences of varying the baseline and gain levels on the response features, such as spike counts (B), peak latency (C) and frequency (D) of the estimated linear filter from the simulated responses, and slope of static nonlinear gain function of the model neuron (E). See Methods for details. *F,G*: Relationship between the magnitudes of the gain modulation and response kinetics modulation by perturbing the histaminergic system for LGN neurons (chemogenetics, red; ciproxifan, green; chlorphenamine, orange; n=300 from 10 animals). Cell types are indicated by different markers (Supplementary Figures 4 and 7). A stronger correlation was found for the peak latencies (F, R = –0.35, p<0.001) than for the peak frequencies (G, Pearson's R = 0.12, p=0.18). Here we combined all data across cell-types and experimental conditions to assess the relationship between the two dependent variables as a result of histamine level manipulations. *H,I*: Corresponding figure panels for RGC responses (n=101 from 11 animals). Significant correlation to the gain modulation was found for the peak latency modulation (R = –0.26, p = 0.03), but not for the peak frequency modulation (R= 0.22, p = 0.11).

Discussion

Here we provide in vivo electrophysiological evidence for histaminergic modulation of the mouse early visual system: the more the histamine released, the slower and weaker the LGN and RGC visual responses in awake head-fixed mice (Figures 1-3). Anterograde tracing of TMN HDC+ neurons confirmed the projection of their axons into the optic chiasm and optic nerve, but not in the retinal tissue (Supplementary Figure 2C-E). Nonetheless, here we used the same mouse lines as previous studies that demonstrated the presence of histaminergic HDC+ axons in the retina (Greferath et al., 2009; Warwick et al., 2024). Moreover, we observed modulation at the level of RGC axons in the optic tract in vivo (Figure 3 and Supplementary Figure 6). It is intriguing that punctate signals of presynaptic markers expressed in TMN HDC+ cells were identified in the optic chiasm (Supplementary Figure 2C), raising a potential role for axonal modulation. However, its contribution should be minimal, if any, because RGC axon potentials should reach the recording site in the optic tract within 1 ms after exiting the eye cup (optic nerve length in mice, <10 mm; conduction velocity, around 10 m/s; Sumitomo et al., 1969). While axonal conduction velocity depends on various factors, including myelination and channel density, its modulation should then occur only on a much shorter time-scale than the observed changes in RGC/LGN response kinetics (up to tens of milliseconds). Taken together, we suggest that the histaminergic modulation likely arises in the retina.

Previous ex vivo studies have reported diverse histaminergic effects in all five major cell types in the retina across species (Vila et al., 2012; Yu et al., 2009, 2011; Horio et al., 2018). Primate RGCs, for instance, either increase or decrease their baseline activity, while their visual responses typically become weaker and slower after histamine application ex vivo (Gastinger et al 2004; Akimov et al., 2010). In contrast, rodent RGCs mostly show an increase in the baseline activity, with various changes in their visual response properties in a histamine dose-dependent manner (Gastinger et al 2004; Warwick et al., 2024). Some of those changes are interrelated: e.g., a broadening of direction-selectivity (DS) tuning can be explained as a

587 natural consequence of the increased baseline activity because a decrease of the DS index
588 (DSI) should follow by definition. Indeed, a reduction of DSI was reported at RGC axon
589 terminals, following an increased baseline activity via arousal or locomotion (Schröder et al.,
590 2020; Liang et al., 2020). However, the mechanisms underlying the histaminergic modulation
591 of the retina remain mostly unclear.

592 We took a computational modelling approach to better understand the net effect of
593 histamine from functional viewpoints (Figure 5), rather than pursuing the underlying
594 biophysical mechanisms. For example, we suggest that the H1 receptors mediate gain
595 modulation in RGCs: chlorphenamine (H1 antagonist) affected the response latency but not
596 the frequency tuning (Figure 3), a distinctive feature of gain modulation identified by our
597 computational modelling analysis (Figure 5). This action of histamine does not have to be
598 directly on RGCs expressing the H1 receptors, but can be mediated indirectly by circuit
599 mechanisms. Indeed, histamine affects both inward and outward currents of amacrine cells in
600 the mouse retina (Horio et al., 2018). The effects of histamine can then be more profound than
601 gain modulation, much as we observed diverse outcomes in RGCs and LGN when different
602 pharmacological and chemogenetic perturbation tools were employed (see also Warwick et
603 al., 2024).

604 Correlation between histamine levels and various behavioral measures has been
605 widely reported (White and Rumbold, 1988; Haas et al., 2008). For instance, the activity of
606 central histaminergic neurons generally follows the circadian rhythm, showing high levels of
607 activity during the active period (i.e., night time for mice as nocturnal animals) and low levels
608 during the sleep period (Mochizuki et al., 1992; Takahashi et al., 2006). Here we performed
609 all our experiments during daytime (ZT4-ZT9). Moreover, the mice remained calm under head
610 fixation, as evidenced by their low spontaneous running behavior (Supplementary Figure 3),
611 following a week of habituation sessions before recordings. The retinal histamine level of the
612 subject mice was then expected to be relatively low during the recordings, given that the
613 mammalian retina contains a comparable level of histamine with other brain areas (around 20-

614 140 ng/g wet tissue, i.e., about 0.1-1 μM; Nowak, 1993). This will explain why we found
615 stronger effects by chemogenetically activating HDC+ neurons in TMN or pharmacologically
616 blocking H3 receptors (mimicking an increase of histamine) than by administering H1
617 antagonists (mimicking a decrease of histamine). However, regulation of the histamine release
618 and metabolism is suggested to be both tissue- and specific-specific (Nowak, 1993): e.g., light
619 stimulation of dark-adapted rabbits at night leads to a substantial reduction of histamine in the
620 retina and the optic nerve (by about 40-50%), but not in other parts of the central nervous
621 system. It is a future challenge to determine the exact level of retinal histamine and its
622 fluctuation under more precisely controlled behavioral contexts.

623 Our observations on the histaminergic effects have certain discrepancies from those
624 reported in previous studies. For example, using the mouse retinal explants, Warwick et al.
625 (2024) showed that histamine increased the baseline activity of RGCs. This effect was dose-
626 dependent, and saturated at 5 μM histamine with an increased baseline firing by ~4 Hz on
627 average. We instead found a reduced firing upon H3 antagonist application or chemogenetic
628 activation of TMN HDC+ cells, while an enhanced firing after blocking H1 receptors (Figure 3
629 and Supplementary Figure 6). This might be because the baseline activity of RGCs in awake
630 mice is already high, by ~20 Hz compared to the ex vivo condition (Boissonnet et al., 2023).
631 Alternatively, the enhancement of the baseline activity in retinal explants could be an artefact
632 of histamine overdose. An isolated retinal tissue should have no baseline histamine because
633 the retina itself does not produce histamine (Gastinger et al., 1999; Greferath et al., 2009).
634 However, bath-application of histamine at the physiological range (0.1-1 μM; Nowak, 1993) or
635 that of H3 antagonists had no effect on the baseline firing ex vivo (Warwick et al., 2024).
636 Moreover, chemogenetic activation of HDC+ axon terminals in retinal explants led to a net
637 reduction of firing, with ~10% of RGCs showing a significant decrease of the baseline firing
638 while only ~1% showing an increase (Warwick et al., 2022). The retinal environment clearly
639 differs between ex vivo and in vivo conditions. One should then be cautious as findings from
640 ex vivo studies may not be directly applicable to the awake, more natural state.

641 What is the biological relevance of histaminergic modulation of the early visual system,
642 starting at the retina? We speculate that species-specific ethological factors play a role. For
643 example, some species may sleep with their eyes open (Rattenborg et al., 2000; Lyamin et
644 al., 2008, 2021; Pigarev et al., 2011), including mice (Yüzgeç et al., 2018; Karimi Abadchi et
645 al., 2020; Turner et al., 2020; Senzai and Scanziani, 2022). Furthermore, as nocturnal animals,
646 mice are less active during daytime. Facilitating visual responses at low histamine level may
647 then be ethologically beneficial for mice to respond faster to visual threats during daytime,
648 especially when mice are less active. In contrast, when animals are more active, other
649 mechanisms, such as arousal, may compensate for the histaminergic effects (Schröder et al.,
650 2020; Liang et al., 2020). Such arguments also hold for those species without eyelids,
651 including some amphibians, reptiles, and fish. To our knowledge, we are the first to report
652 histaminergic effects on LGN in awake mice. Recordings from LGN in cats and guinea pigs
653 (under the anesthetized condition or brain slices; McCormick and Williamson, 1991; Uhlrich,
654 et al., 2002) suggest that histamine leads to a slow depolarization of the relay cells, enhancing
655 the baseline activity but introducing a lag in their visual responses. However, substantial
656 differences exist in the early visual processing between awake and anesthetized conditions
657 (Durand et al., 2016; Boissonnet et al., 2023). Further studies are needed to address how
658 histamine affects visual processing and perception in awake animals in tissue- and species-
659 specific manners.

660 Growing evidence supports significant correlations between awake retinal responses
661 and various behavioral measures, such as pupil dynamics and locomotion (Schröder et al.,
662 2020; Liang et al., 2020; Boissonnet et al., 2023). Such correlations were also found in our
663 data sets; however, we demonstrated that an animal's pupil dynamics and locomotion
664 behavior have little to do with the observed histaminergic effects on RGC/LGN responses
665 (Figure 4 and Supplementary Figures 3 and 10). This indicates that mechanisms other than
666 histamine are involved in the retinal modulation by arousal and locomotion. The retina exploits
667 not just histamine but also many other neuromodulators, synthesized inside (Pourcho, 1996)

668 or outside the retina (Koves et al., 2016; Vereczki et al., 2024), such as the centrifugal
669 serotonergic system (Schütte, 1995; Repérant et al., 2000; Gastinger et al., 2006). It is a future
670 challenge to identify what behavior is controlled by histamine and vice versa, and characterize
671 the anatomical and physiological features of those HDC+ cells projecting to the retina to clarify
672 behavioral relevance of the histaminergic modulation of the early visual system.

673 Materials and Methods

674 No statistical method was used to predetermine the sample size. The significance level was
675 0.05 (with multiple comparison correction where appropriate) in all analyses unless noted
676 otherwise. All experiments were performed under the license 233/2017-PR and 220/2024-PR
677 from the Italian Ministry of Health, following protocols approved by the Institutional Animal
678 Care and Use Committee at European Molecular Biology Laboratory. The data analyses were
679 done in Python and Matlab.

680 Animals

681 Animals were housed on a 12h light-dark cycle, with ad libitum access to water and food. All
682 experiments were performed on female mice. A total of 22 wild-type (C57BL6/J;
683 RRID:IMSR_JAX:000664) and 12 hemizygous HDC-Cre (Hdctm1.1(icre)Wwis/J;
684 RRID:IMSR_JAX:021198) mice were used for pharmacological and chemogenetic
685 manipulations, respectively. Additional 9 hemizygous HDC-Cre mice were used for
686 anterograde tracing of HDC+ cells in TMN.

687 Surgical procedures

688 All surgical procedures were performed in animals from 4 to 19 weeks old (9.2 weeks median
689 age). Before the surgery, animals were injected with Carprofen (5 mg/kg) and then
690 anaesthetized with isoflurane (4% for induction, 1% for maintenance in O_2). Throughout the
691 surgery, the temperature of the animals was kept stable at 37°C using a heating pad
692 (Supertech Physiological). Ointment (VitA-Pos, Ursapharm) was applied on both eyes to

693 prevent them from drying during the surgery, and the animals were placed in a stereotaxic
694 frame (Stoelting 51625). A portion of the scalp was removed to expose the skull and the
695 periosteum was scraped away with a round scalpel to increase adherence of the dental
696 cement. For those mice belonging to the chemogenetic manipulation group, the skull was
697 aligned to level bregma and lambda on the same horizontal plane, and a 100 μm craniotomy
698 was performed using a motorized drill attached to the stereotaxic arm. Viral solution (250 nL;
699 AAV9::FLEX-PSAM Y115F,L141F:5HT3 HC; Vector Biolabs, VB773) was injected with an
700 automatic injector pump at 1 nL/sec, at [-2.6, ±0.8, -5.3] or [-1.7, ±0.5, -5.3] in [Anterior-
701 Posterior (AP), Medial-Lateral (ML), Dorsal-Ventral (DV)] coordinates for targeting TMN and
702 non-TMN areas of the hypothalamus, respectively. All animals were then implanted with a
703 custom-made titanium head plate, cemented on the skull using a mixture of cyanoacrylate
704 (Loctite 401, Henkel) and dental cement (Paladur, Kulzer). The head plate featured a hole (8
705 mm diameter), allowing for clear observation of both bregma and lambda. The skull surface
706 was then glazed with a thick layer of cyanoacrylate to support the skull with mechanical,
707 atmospheric and biological protection, while still allowing for visual identification of reference
708 points. After the surgery animals were allowed to recover on a heating pad and then housed
709 in individual cages. During the following seven days, the mice were administered with
710 analgesia (Carprofen; 50 mg/mL) diluted in the drinking water.

711 Anterograde tracing

712 For anterograde tracing of HDC+ cells, we injected recombinant AAVs carrying Cre-dependent
713 fluorescent markers (100 nL; rAAV9::CAG-FLEX-Synaptophysin-GFP or AAV2/1::CAG-
714 FLEX-axon-GFP) into the TMN of HDC-Cre mice (n=9) as described above. At least 10 days
715 after the injection, the animals were anesthetized (2.5% Avertin, 16 μL/g, intraperitoneal
716 injection) and perfused with paraformaldehyde (PFA; 4% in phosphate buffer solution). The
717 brain tissues including the optic chiasms and optic nerves were dissected and post-fixed
718 overnight in 4% PFA at 4°C. Coronal sections of the brain tissue (thickness, 80 μm) were then

examined under a laser scanning confocal microscope (Leica TCS SP5; Supplementary Figure 2).

In vivo electrophysiology

After recovery from the surgery, animals were habituated to head fixation by placing them in the experimental apparatus over the course of one week, twice a day for up to two hours. On the day of the recording, we first placed the subject animal in the recording set up with its head fixed, and determined the electrode penetration path to the target area (optic tract, [-1.34, +1.87, +4.74], [-1.70, +1.87, +4.74], or [-1.82, +2.35, +4.07] in [AP, ML, DV] coordinates; LGN, [-2.3, +2.3, +2.8]) using the robotic stereotaxic system (StereoDrive, NeuroStar). The animal was then briefly anesthetized (with isoflurane for about 5 minutes) and a hole was drilled around the electrode entry point on the skull. After the removal of the anesthesia, an acute silicone probe (Buzsaki32L, Neuronexus; or P2, Cambridge Neurotech) coated with a fluorescent dye (DiI stain, Invitrogen, D282) was lowered at 5 μm/s using the robotic arm until visual responses were found in the target area. All recordings were done during the day time (between 11am/ZT4 and 4pm/ZT9; 1pm/ZT6 ± 1 hour, mean ± standard deviation; 96% of the paired recordings were conducted within 2 hours of each other).

After presenting a battery of visual stimuli, we briefly anesthetized the animal with isoflurane and intraperitoneally injected 0.9% saline solution alone or that containing chlorphenamine (H1 antagonist, 5 mg/kg; Frisch et al., 1997; Valle-Baurista et al. 2022), ciproxifan (H3 antagonist, 12 mg/kg; Browman et al., 2004; Muindi et al., 2015), or PSEM (5 mg/kg; Magnus et al., 2011). About 20 minutes after the injection and removal of the anesthesia, we presented the same battery of visual stimuli to the animal for the second recording session. Here we did not target the H2 or H4 receptors because blocking the H2 receptors has little effect on retinal physiology ex vivo (Warwick et al., 2024), and the functional role of the H4 receptors in the central nervous system remains unclear (Strakhova et al., 2009). In our electrophysiology experiments, we could not keep the same cells long enough to test if the effects of these manipulations were reversible or not.

After all the recording sessions, the electrode position was verified histologically (e.g., Figures 1B, LGN; Figure 3B, optic tract). After retracting the silicon probe, the mice were anesthetized (2.5% Avertin, 16 µL/g, intraperitoneal injection) and perfused with 4% PFA. The brain tissue was harvested and post-fixed overnight in 4% PFA at 4°C. Coronal sections of the brain tissue (thickness, 100-150 µm) were then examined under a fluorescence microscope (Leica, LMD7000 with N2.1 filter cube) to visualize the trace left by the DiI stain on the probe. To examine the PSAM expression, staining of the slices was performed (Supplementary Figure 2A,B): primary staining, 1-hour-incubation with an alpha-bungarotoxin/biotin-XX conjugate (ThemoFisher, B1196) diluted with PBS with 0.1% Tween (1/500) at room temperature; secondary staining, streptavidin and alexa-fluorophore, 1/500 in PBS(T) 0.1% for 2 hours at room temperature.

Visual stimulation

Visual stimuli were presented as described before (Boissonnet et al., 2023). Briefly, visual stimuli were projected onto a spherical screen (20cm in radius) painted with ultra-violet (UV) reflective white paint, placed 20 cm from the mouse's left eye. A gamma-corrected digital light processing device (DLP, Texas Instruments, DLPDLCR3010EVM-LC) was used as a light source after the green and the red light-emitting diodes (LEDs) were replaced with UV (365nm, LZ1-00UV00, LED Engine) and infrared (IR; 950nm, SFH 4725S, Osram) LEDs, respectively. The IR light was used as a synchronization signal and recorded with a photodiode (PDA100A2, Thorlabs). Stimulation was conducted at 60 frames per second (FPS), and covered 73° in azimuth and 44° in altitude from the mouse eye position. The maximum light intensity at the eye position was 31 mW/m^2 (15.4 mW/m^2 for UV LED and 15.9 mW/m^2 for blue LED; measured with S121C sensor, Thorlabs), leading to mesopic to photopic conditions. We presented the following stimuli using QDSpy: a randomly flickering full-field stimulus (5 minutes), consisting of a random sequence of black and white frames at 60 FPS; a black-and-white binary dense noise stimulus (15 minutes), consisting of a 32-by-18 pixels checkerboard, where each pixel followed an independent random sequence at 60 FPS but the overall

luminance of the frame was kept constant at the mean value; a moving grating stimulus in eight different directions (spatial frequencies of square waves, 3° or 20°; moving speed, 7.5°/s or 15°/s); full-field contrast-inverting stimuli in an "OFF-ON-OFF" sequence at maximum contrast (2 s each), followed by a sinusoid (1.5 Hz) with a linearly increasing amplitude from 0% to 100% contrast over 10 s (10 trials) or a sequence of sinusoids with different temporal frequencies (1.875, 3.75 and 7.5 Hz, each for 2 s; 15 and 30 Hz for 1 s) at maximum contrast (10 trials), with an inter-trial interval of 1 s (gray screen).

Electrophysiology data analysis

Here we adapted previously established methods of spiking sorting and optic tract data analysis (Boissonnet et al., 2023). In brief, we first concatenated the raw data from the same animal before and after treatment into a single binary file, and used Kilosort 2.0 to sort spikes with a set of default parameters, except for the spike detection threshold to be 6 during optimization. Single-units were then identified by clustering in principal component space using Phy for visualization and manual data curation. Only those units that maintained the average spike waveforms and autocorrelograms with a minimal refractory period of 1 ms were kept for subsequent analyses (Supplementary Figure 1). Specifically, we selected RGCs/LGN cells as those with robust visual responses: i.e., $\mathrm{SNR} = \mathrm{var}[\langle r(t)\rangle]_t / \langle \mathrm{var}[r(t)]_t \rangle > 0.15$, where $r(t)$ is the response during the "ON-OFF" part of the OFF-ON-OFF stimulus sequence, $\langle\cdot\rangle$ indicates the mean over trials, and $\mathrm{var}[\cdot]_t$ the variance over time t (bin size, 1/60 ms), respectively; and the estimated temporal filter should have $p < 10^{-10}$ in at least one time bin within 200 ms from the spike onset (see below for details). Single-units with little or no visual responses were excluded from the analysis as non-target cells, such as the axons from the parabigeminal nucleus in the optic tract (Tokuoka et al., 2020; Reinhard et al., 2019). In total, we obtained 337 RGCs from 20 animals and 557 cells in LGN from 14 mice. These RGCs typically had a triphasic spike waveform as expected for axonal signals (Barry, 2015).

To characterize the peak latency and firing rate of the responses to full-field contrast-inverting stimuli (Figure 1 and Supplementary Figure 6), we first identified the cell's response preference to stimulus polarity using an ON-OFF index defined as $(r_{\mathrm{ON}} - r_{\mathrm{OFF}})/(r_{\mathrm{ON}} + r_{\mathrm{OFF}})$, where r_{ON} and r_{OFF} are the mean firing rate during the ON and the second OFF periods of the OFF-ON-OFF stimulus sequence. We then computed the peri-stimulus time histogram (bin size, 1 ms), smoothed it with a Gaussian filter (kernel width, 6 standard deviation), and identified the first peak upon stimulus onset or offset for those cells with positive or negative ON-OFF index values, respectively. We then performed pairwise comparisons on the peak latencies and firing rates before and after each treatment (e.g., Figure 1F-J). To compare the changes in the detected peak latency and firing rates across different conditions (e.g., Figure 1K,L), we performed Kruskal-Wallis test on a modulation index defined as $(a_{\mathrm{after}} - a_{\mathrm{before}})/(a_{\mathrm{after}} + a_{\mathrm{before}})$, where a is either the detected peak latency or peak firing rate before and after treatment.

For systematically characterizing the visual response properties, we used stimulus ensemble statistical techniques (reverse correlation methods; 500 ms window; Δt = 1/60 s bin size) to calculate the linear filter and static nonlinear gain function of the recorded cells in response to white-noise stimuli as described before (Figure 2B; Boissonnet et al., 2023). Briefly, we first obtained the linear filter of each cell by calculating a spike-triggered average (STA) of the stimulus with ±1 being "white" and "black," respectively, under a given behavioral state (e.g., when the animal stayed stationary below 2 cm/s). As a quality measure, p-value was computed for each time bin against a null hypothesis that the STA follows a normal distribution with a mean of zero and a variance of $1/C$, where C is the total number of spikes. As a measure of the cell's response kinetics, we then estimated the peak latency by fitting a difference-of-Gaussian curve to the linear filter; and the spectral peak frequency by the Fourier analysis on the linear filter. The ON-OFF polarity index of a temporal filter was defined as the difference of its peak and valley, divided by the sum of the two (Figure 4G and Supplementary Figure 10D). Spatial response properties were examined for STAs from "checkerboard"

stimulation, using the time window where the eye position remained within 1 inter-quartile range in both horizontal and vertical coordinates for at least 2 seconds (Supplementary Figures 5C and 8A) to minimize the effects of eye movements while retaining enough data for RF estimation. In particular, we fitted a two-dimensional Gaussian envelope to the spatial filter at the peak latency (e.g., Supplementary Figure 5D), and the receptive field (RF) size was estimated as twice the mean standard deviation (SD) of the long and short axes. Modulation index was used to characterize the change in a response feature before and after treatment, such as the peak latency and frequency, the mean firing rate, and the receptive field size (Figures 2K-N, 3K-N). Here we focused only on those data when the mouse stayed stationary (<2 cm/s) to minimize the side effects of locomotion behaviour (Erisken et al., 2014; Schröder et al., 2020; Supplementary Figure 3).

The linear temporal filters from full-field white-noise stimuli were used for broadly classifying the response types of RGCs and LGN cells, respectively (Supplementary Figures 4A,B and 7A,B). Specifically, we first used t-Distributed Stochastic Neighbor Embedding (t-SNE) to map the STAs onto two-dimensional space, and then used K-means++ algorithm for heuristically categorizing the responses into the following six types: fast ON, ON, slow ON, fast OFF, OFF, and slow OFF. Our data sets were not large enough to physiologically classify and identify all the cell types reported thus far (Baden et al., 2016; Rosón et al., 2019). Direction-selectivity (DS) and orientation-selectivity (OS) indices were calculated by projecting the responses to the moving grating stimuli in eight different directions onto a complex exponential: $\mathrm{DS/OS\ index} = \left\| \sum_k e^{-i\alpha\omega_k} / \sum_k r_k \right\|$, where ω_k and r_k are the angle of the k-th direction and the cell's corresponding responses, respectively; and $\alpha = 1$ and 2 for the DS and OS indices, respectively (Supplementary Figure 9).

Static nonlinear gain function of each cell (bin size, 0.1) was computed as: P(response | stimulus) = N(stimulus | response) / N(stimulus) / Δt, where N(stimulus | response) and N(stimulus) are the distributions of spike-triggered stimulus ensembles projected onto the L2-normalized STA and the entire stimulus ensembles, respectively. The ratio of P(response |

stimulus) before and after the treatment was used as a measure of response gain modulation for each cell.

Behavioral data analysis

For all experiments, the animal's left eye – i.e., the side presented with visual stimuli – was recorded using an IR camera (The Imaging Source, DMK23UV024) to monitor its motion and pupil dynamics at 30-60Hz. Pupil detection was done using a Mask-Region based Convolutional Neural Network (Mask-RCNN), trained as described previously (Boissonnet et al., 2023). A two-dimensional ellipse was fit to the pupil, and the large axis diameter was used as a measure of the pupil size, normalized by the median value before treatment for each animal (Figure 4A). To examine the pupil size effects on the response dynamics, a threshold at 33 and 66 percentiles was used to define constricted, neutral, and dilated pupil period, respectively. To examine the effects of the pupil dynamics, we took the time derivative of the pupil size dynamics, and set a threshold at ±0.01 point per second to define constricting, stable, and dilating pupil periods, respectively.

We also monitored the running speed of an animal based on the turning speed of the custom-made rotary treadmill throughout the recordings. We set a threshold at 2 cm/s to detect running behavior (Supplementary Figure 3A). For quantification, we measured the fraction of the running period (Supplementary Figure 3B), and the median running speed when mice moved at >2 cm/s before and after each treatment (Supplementary Figure 3C)..

Model analysis

To explore how different aspects of neuronal intrinsic properties and output responses are interrelated between each other, we simulated a model neuron's responses to white-noise stimuli using different model parameter values (Figure 5A), and characterized these simulated responses using a linear-nonlinear cascade model as we did for the experimental data.

Specifically, we employed an integrate-and-fire neuron model with Poisson spiking and refractoriness. A model neuron's discrete linear filter (of length $n_T = 25$) was given by a trigonometric function with logarithmic scale in time: i.e., $L(i) = \sin[2\pi(10^{t_i} - 1)/(10^{s_t} - 1)]$, where $s_t = 1.5$ is a temporal spacing parameter and $t_i = i \cdot s_t/(n_T - 1)$ for $i = 0, \ldots, n_T - 1$. The spike-generating function $V(i)$ was then modelled by first projecting the white-noise Gaussian stimulus $S(i)$ (of length 1,000,000; normalized to have a maximum value of 1) onto $L(i)$, followed by the addition of baseline B and the multiplication by gain G: i.e., $V(i) = G \cdot \left(\sum_j L(j) \cdot S(i-j) + B\right)$. For each simulation, we chose the value of B from -0.45 to $+0.45$ in steps of 0.15; and that of G from 1.2^g with $g = -3, \ldots, +3$. The spiking response was then generated by thresholding $V(i)$(at a random threshold for every time point derived from a uniform distribution from 0 to 1) and refractoriness (given by an exponential filter: $-\exp[-i/s_h]$ for $i = 0, \ldots, 5$ with $s_h = 1$). The output spike trains were then subject to the reverse-correlation analysis as described above to characterize the apparent linear filter and static nonlinearity of the model neuron, much as we did for the experimentally recorded RGCs and LGN cells. Specifically, we focused on the peak latency and frequency of the estimated linear filters and the slope of the estimated static nonlinear gain function, and examined how these features depended on the baseline B and the intrinsic gain G of the model neuron to provide a minimal phenomenological explanation to our observations (Figure 5B-E).

Acknowledgments

This work was supported by research grants from EMBL (H.A.). The EMBL Advanced Light Microscopy Facility are acknowledged for support in histological image acquisition and analyses, and EMBL IT Support for provision of computer and data storage servers. We thank Dmitry Molotkov, Tom Boissonnet, Vanesa Pelcastre, Sahana Rao, Shabnam Chandel, Lily Knowles for their help in experiments, and all the Asari lab members for many useful discussions.

References

Akimov, N.P., Marshak, D.W., Frishman, L.J., Glickman, R.D., Yusupov, R.G. (2010). Histamine Reduces Flash Sensitivity of ON Ganglion Cells in the Primate Retina. Invest Ophthalmol Vis Sci. 51(7), 3825–3834.

Baden, T., Berens, P., Franke, K., Rosón, M. R., Bethge, M., Euler, T. (2016). The functional diversity of retinal ganglion cells in the mouse. Nature, 529(7586), 345-350.

Barry, J.M. (2015). Axonal activity in vivo: technical considerations and implications for the exploration of neural circuits in freely moving animals. Front. Neurosci. 9, 153.

Bloomfield, S.A., Völgyi, B. (2009). The diverse functional roles and regulation of neuronal gap junctions in the retina. Nat Rev Neurosci. 10(7), 495–506.

Boissonnet, T., Tripodi, M., Asari, H. (2023). Awake responses suggest inefficient dense coding in the mouse retina. Elife. 12, e78005.

Browman, K.E., Komater, V.A., Curzon, P., Rueter, L.E., Hancock, A.A., Decker, M.W., Fox, G.B. (2004). Enhancement of prepulse inhibition of startle in mice by the H3 receptor antagonists thioperamide and ciproxifan. Behav Brain Res 153(1), 69-76.

Brown, R.E., Sergeeva, O.A., Eriksson, K.S., Haas, H.L. (2002). Convergent Excitation of Dorsal Raphe Serotonin Neurons by Multiple Arousal Systems (Orexin/Hypocretin, Histamine and Noradrenaline). J. Neurosci. 22, 8850–8859.

Dipoppa, M., Ranson, A., Krumin, M., Pachitariu, M., Carandini, M., Harris, K.D. (2018). Vision and Locomotion Shape the Interactions between Neuron Types in Mouse Visual Cortex. Neuron 98(3), 602–615.e8.

Durand, S., Iyer, R., Mizuseki, K., de Vries, S., Mihalas, S., Reid, R. C. (2016). A Comparison of Visual Response Properties in the Lateral Geniculate Nucleus and Primary Visual Cortex of Awake and Anesthetized Mice. J Neurosci, 36(48), 12133–12156.

925 Erisken, S., Vaiceliunaite, A., Jurjut, O., Fiorini, M., Katzner, S., Busse, L. (2014). Effects
926 of locomotion extend throughout the mouse early visual system. Curr Biol, 24(24), 2899–
927 2907.

928 Esbenshade, T.A., Krueger, K.M., Miller, T.M., Kang, C.H., Denny, L.I., Witte, D.G., Yao,
929 B.B., Fox, G.B., Faghih, R., Bennani, Y.L., Williams, M., Hancock, A.A. (2003). Two novel
930 and selective nonimidazole histamine H3 receptor antagonists A-304121 and A-317920: I.
931 In vitro pharmacological effects. J Pharmacol Exp Ther 305(3), 887–896.

932 Esposti, F., Johnston, J., Rosa, J. M., Leung, K.-M., Lagnado, L. (2013). Olfactory
933 Stimulation Selectively Modulates the OFF Pathway in the Retina of Zebrafish. Neuron,
934 79(1), 97-110.

935 Fang, S.Y., Druce, H.M., Baraniuk, J.N. (1998). Anticholinergic properties of
936 brompheniramine, chlorpheniramine, and atropine in human nasal mucosa in vitro. Am J
937 Rhinol 12(2), 131–133.

938 Frisch, C., Hasenöhrl, R.U., Huston, J.P. (1997). The histamine H1-antagonist
939 chlorpheniramine facilitates learning in aged rats. Neurosci Lett 229(2), 89–92.

940 Gastinger, M.J., O'Brien, J.J., Larsen, J.N.B., Marshak, D.W. (1999). Histamine
941 Immunoreactive Axons in the Macaque Retina. Invest. Ophthalmol. Vis. Sci. 40, 487–495.

942 Gastinger, M. J., Tian, N., Horvath, T., Marshak, D. W. (2006). Retinopetal axons in
943 mammals: Emphasis on histamine and serotonin. Curr. Eye Res. 31, 655–667.

944 Goel, M., Mangel, S.C. (2021). Dopamine-Mediated Circadian and Light/Dark-Adaptive
945 Modulation of Chemical and Electrical Synapses in the Outer Retina. Front Cell Neurosci
946 15, 647541.

947 Greferath, U., Kambourakis, M., Barth, C., Fletcher, E.L., Murphy, M. (2009).
948 Characterization of histamine projections and their potential cellular targets in the mouse
949 retina. Neuroscience 158, 932–944.

950 Grozdanic, S., Betts, D.M., Allbaugh, R.A., Sakaguchi, D.S., Kwon, Y.H., Kardon, R.H.,
951 Sonea, I.M. (2003). Characterization of the pupil light reflex, electroretinogram and
952 tonometric parameters in healthy mouse eyes. Curr Eye Res 26(6), 371–378.

953 Haas, H., Panula, P. (2003). The role of histamine and the tuberomamillary nucleus in the
954 nervous system. Nat. Rev. Neurosci. 4, 121–130.

955 Haas, H.L., Sergeeva, O.A., Selbach, O. (2008). Histamine in the nervous system. Physiol
956 Rev 88(3), 1183–1241.

957 Hagenow, S., Stasiak, A., Ramsay, R.R., Stark, H. (2017). Ciproxifan, a histamine H3
958 receptor antagonist, reversibly inhibits monoamine oxidase A and B. Sci Rep 7, 40541.

959 Horio, K., Ohkuma, M., Miyachi, E.-I. (2018). The effect of histamine on inward and
960 outward currents in mouse retinal amacrine cells. Cell. Mol. Neurobiol. 38, 757–767.

961 Jacoby, J., Nath, A., Jessen, Z.F., Schwartz, G.W. (2018). A Self-Regulating Gap Junction
962 Network of Amacrine Cells Controls Nitric Oxide Release in the Retina. Neuron 100, 1149-
963 1162.e5.

964 John, J., Wu, M.-F., Boehmer, L.N., Siegel, J.M. (2004). Cataplexy-Active Neurons in the
965 Hypothalamus: Implications for the Role of Histamine in Sleep and Waking Behavior.
966 Neuron 42, 619–634.

967 Kamei, C., Okumura, Y., Tasaka, K. (1993). Influence of histamine depletion on learning
968 and memory recollection in rats. Psychopharmacology (Berl.) 111, 376–382.

969 Karimi Abadchi, J., Nazari-Ahangarkolaee, M., Gattas, S., Bermudez-Contreras, E.,
970 Luczak, A., McNaughton, B.L., Mohajerani, M.H. (2020) Spatiotemporal patterns of
971 neocortical activity around hippocampal sharp-wave ripples. Elife 9, e51972.

972 Khateb, A., Fort, P., Pegna, A., Jones, B.E., Mühlethaler, M. (1995). Cholinergic nucleus
973 basalis neurons are excited by histamine in vitro. Neuroscience 69, 495–506.

Khouma, A., Moeini, M.M., Plamondon, J., Richard, D., Caron, A., Michael, N.J. (2023). Histaminergic regulation of food intake. Front. Endocrinol. 14.

Klapdor, K., Hasenöhrl, R.U., Huston, J.P. (1994). Facilitation of learning in adult and aged rats following bilateral lesions of the tuberomammillary nucleus region. Behav. Brain Res. 61, 113–116.

Koves, K., Csaki, A., Vereczki, V. (2016). Recent Research on the Centrifugal Visual System in Mammalian Species. Anat Physiol 6(3), 216.

Labandeira-Garcia, J.L., Guerra-Seijas, M.J., Gonzalez, F., Perez, R., Acuña, C., (1990). Location of neurons projecting to the retina in mammals. Neurosci. Res. 8, 291–302.

Lee, S.-H., Dan, Y. (2012). Neuromodulation of Brain States. Neuron 76, 209–222.

Liang, L., Fratzl, A., Reggiani, J.D.S., El Mansour, O., Chen, C., Andermann, M.L. (2020). Retinal Inputs to the Thalamus Are Selectively Gated by Arousal. Curr. Biol. CB 30, 3923–3934.e9.

Lin, W., Xu, L., Zheng, Y., An, S., Zhao, M., Hu, W., Li, M., Dong, H., Li, A., Li, Y., Gong, H., Pan, G., Wang, Y., Luo, Q., Chen, Z. (2023) Whole-brain mapping of histaminergic projections in mouse brain. Proc. Natl. Acad. Sci. U. S. A. 120, e2216231120.

Liu, Y., Rodenkirch, C., Moskowitz, N., Schriver, B., Wang, Q. (2017). Dynamic Lateralization of Pupil Dilation Evoked by Locus Coeruleus Activation Results from Sympathetic, Not Parasympathetic, Contributions. Cell Rep, 20(13), 3099–3112.

Lyamin, O.I., Manger, P.R., Ridgway, S.H., Mukhametov, L.M., Siegel, J.M. (2008). Cetacean sleep: an unusual form of mammalian sleep. Neurosci Biobehav Rev 32(8), 1451–1484.

Lyamin, O.I., Siegel, J.M., Evsigneev, R.V., Nazarenko, E.A., Rozhnov, V.V. (2021). Characteristics of Sleep-Wakefulness Cycle and Circadian Activity in the Lesser Mouse-Deer (Tragulus kanchil). Dokl Biol Sci 500(1), 153–158.

Magnus, C.J., Lee, P.H., Bonaventura, J., Zemla, R., Gomez, J.L., Ramirez, M.H., Hu, X., Galvan, A., Basu, J., Michaelides, M., Sternson, S.M. (2019). Ultrapotent chemogenetics for research and potential clinical applications. Science. 364(6436), eaav5282

McCormick, D.A., Nestvogel, D.B., He, B.J., (2020). Neuromodulation of brain state and behaviour. Ann. Rev. Neurosci. 43(1), 391–415.

McCormick, D.A., Williamson, A. (1991). Modulation of neuronal firing mode in cat and guinea pig LGNd by histamine: possible cellular mechanisms of histaminergic control of arousal. J. Neurosci. 11 (10), 3188–3199.

Mochizuki, T., Yamatodani, A., Okakura, K., Horii, A., Inagaki, N., Wada, H. (1992). Circadian rhythm of histamine release from the hypothalamus of freely moving rats. Physiol. Behav. 51, 391–394.

Muindi, F., Colas, D., Ikeme, J., Ruby, N.F., Heller, H.C. (2015). Loss of Melanopsin Photoreception and Antagonism of the Histamine H3 Receptor by Ciproxifan Inhibit Light-Induced Sleep in Mice. PLoS One 10(6), e0128175.

Niell, C.M., Stryker, M.P. (2010). Modulation of visual responses by behavioral state in mouse visual cortex. Neuron 65(4), 472–479.

Nowak, J.Z. (1993). Histamine in the retina and some other components of the visual system. Prog Retin Res 12, 41–74.

Orsetti, M., Ghi, P., Carlo, G.D. (2001). Histamine H3-receptor antagonism improves memory retention and reverses the cognitive deficit induced by scopolamine in a two-trial place recognition task. Behav. Brain Res. 124, 235–242.

Parmentier, R., Ohtsu, H., Djebbara-Hannas, Z., Valatx, J.-L., Watanabe, T., Lin, J.-S. (2002). Anatomical, Physiological, and Pharmacological Characteristics of Histidine Decarboxylase Knock-Out Mice: Evidence for the Role of Brain Histamine in Behavioral and Sleep–Wake Control. J. Neurosci. 22, 7695–7711.

1024 Pigarev, I.N., Fedorov, G.O., Levichkina, E.V., Marimon, J.M., Pigareva, M.L., Almirall, H.
1025 (2011). Visually triggered K-complexes: a study in New Zealand rabbits. Exp Brain Res
1026 210(1), 131–142.

1027 Pourcho, R.G. (1996). Neurotransmitters in the retina. Curr Eye Res 15(7), 797–803.

1028 Rattenborg, N.C., Amlaner, C.J., Lima, S.L. (2000). Behavioral, neurophysiological and
1029 evolutionary perspectives on unihemispheric sleep. Neurosci Biobehav Rev 24(8), 817–
1030 842.

1031 Reggiani, J.D.S., Jiang, Q., Barbini, M., Lutas, A., Liang, L., Fernando, J., Deng, F., Wan,
1032 J., Li, Y., Chen, C., Andermann, M.L. (2023). Brainstem serotonin neurons selectively gate
1033 retinal information flow to thalamus. Neuron 111, 711–726.e11.

1034 Reinhard, K., Li, C., Do, W., Burke, E.G., Heynderickx, S., Farrow, K. (2019). A projection
1035 specific logic to sampling visual inputs in mouse superior colliculus. eLife 8, e50697.

1036 Repérant, J., Médina, M., Ward, R., Miceli, D., Kenigfest, N.B., Rio, J.P., Vesselkin, N.P.
1037 (2007). The evolution of the centrifugal visual system of vertebrates. A cladistic analysis
1038 and new hypotheses. Brain Res. Rev. 53, 161–197.

1039 Repérant, J., Araneda, S., Miceli, D., Medina, M., Rio, J. P. (2000). Serotonergic
1040 retinopetal projections from the dorsal raphe nucleus in the mouse demonstrated by
1041 combined [3H] 5-HT retrograde tracing and immunolabeling of endogenous 5-HT. Brain
1042 Res. 878, 213–217.

1043 Rosón, M.R., Bauer, Y., Kotkat, A.H., Berens, P., Euler, T., Busse, L. (2019). Mouse dLGN
1044 Receives Functional Input from a Diverse Population of Retinal Ganglion Cells with Limited
1045 Convergence. Neuron 102(2), 462-476.e8.

1046 Rubio, S., Begega, A., Santin, L.J., Arias, J.L. (2002). Improvement of spatial memory by
1047 (R)-α-methylhistamine, a histamine H3-receptor agonist, on the Morris water-maze in rat.
1048 Behav. Brain Res. 129, 77–82.

1049 Savier, E.L., Chen, H., Cang, J. (2019). Effects of Locomotion on Visual Responses in the
1050 Mouse Superior Colliculus. J Neurosci 39(47), 9360–9368.

1051 Scammell, T.E., Jackson, A.C., Franks, N.P., Wisden, W., Dauvilliers, Y. (2018).
1052 Histamine: neural circuits and new medications. Sleep 42, zsy183.

1053 Schröder, S., Steinmetz, N.A., Krumin, M., Pachitariu, M., Rizzi, M., Lagnado, L., Harris,
1054 K.D., Carandini, M. (2020). Arousal Modulates Retinal Output. Neuron 107, 487–495.e9.

1055 Schütte, M. (1995). Centrifugal innervation of the rat retina. Vis. Neurosci. 12, 1083–1092.

1056 Senzai, Y., Scanziani, M. (2022) A cognitive process occurring during sleep is revealed by
1057 rapid eye movements. Science 377, 999–1004.

1058 Strakhova, M.I., Nikkel, A.L., Manelli, A.M., Hsieh, G.C., Esbenshade, T.A., Brioni, J.D.,
1059 Bitner, R.S. (2009) Localization of histamine H4 receptors in the central nervous system
1060 of human and rat. Brain Res, 1250, 41-48.

1061 Sumitomo, I., Ide, K., Iwama, K., Arikuni, T. (1969). Conduction velocity of optic nerve
1062 fibers innervating lateral geniculate body and superior colliculus in the rat. Exp Neurol
1063 25(3), 378–392.

1064 Takahashi, K., Lin, J.-S., Sakai, K. (2006). Neuronal activity of histaminergic
1065 tuberomammillary neurons during wake-sleep states in the mouse. J. Neurosci. Off. J. Soc.
1066 Neurosci. 26, 10292–10298.

1067 Thakkar, M.M. (2011). Histamine in the regulation of wakefulness. Sleep Med Rev. 15(1),
1068 65-74.

1069 Tokuoka, K., Kasai, M., Kobayashi, K., Isa, T. (2020). Anatomical and electrophysiological
1070 analysis of cholinergic inputs from the parabigeminal nucleus to the superficial superior
1071 colliculus. J Neurophysiol. 124(6), 1968–1985.

1072 Turner, K.L., Gheres, K.W., Proctor, E.A., Drew, P.J. (2020). Neurovascular coupling and
1073 bilateral connectivity during NREM and REM sleep. Elife 9, e62071.

1074 Uhlrich, D. J., Manning, K. A., Xue, J.-T.. (2002). Effects of activation of the histaminergic
1075 tuberomammillary nucleus on visual responses of neurons in the dorsal lateral geniculate
1076 nucleus. J. Neurosci. 22, 1098–1107.

1077 Valdés, J.L., Sánchez, C., Riveros, M.E., Blandina, P., Contreras, M., Farías, P., Torrealba,
1078 F. (2010). The histaminergic tuberomammillary nucleus is critical for motivated arousal.
1079 Eur. J. Neurosci. 31, 2073–2085.

1080 Valle-Bautista, R., Márquez-Valadez, B., Herrera-López, G., Griego, E., Galván, E.J., Díaz,
1081 N.-F., Arias-Montaño, J.-A., Molina-Hernández, A. (2022). Long-Term Functional and
1082 Cytoarchitectonic Effects of the Systemic Administration of the Histamine H1 Receptor
1083 Antagonist/Inverse Agonist Chlorpheniramine During Gestation in the Rat Offspring
1084 Primary Motor Cortex. Front Neurosci 15, 740282.

1085 Vereczki, V., Köves, K., Csáki, A. (2024). Current state of knowledge on the centrifugal
1086 visual system (including the pinealo-to-retinal connection) in mammals and its
1087 hypothesized role in circadian rhythms. Explor Neurosci, 3, 51–64.

1088 Vila, A., Satoh, H., Rangel, C., Mills, S.L., Hoshi, H., O'Brien, J., Marshak, D.R., Macleish,
1089 P.R., Marshak, D.W. Histamine receptors of cones and horizontal cells in Old World
1090 monkey retinas. J Comp Neurol. 520(3), 528–543.

1091 Wang, Y.-Q., Li, R., Wu, X., Zhu, F., Takata, Y., Zhang, Z., Zhang, M.-Q., Li, S.-Q., Qu,
1092 W.-M. (2015). Fasting activated histaminergic neurons and enhanced arousal effect of
1093 caffeine in mice. Pharmacol. Biochem. Behav. 133, 164–173.

1094 Warwick, R.A., Riccitelli, S., Heukamp, A.S., Yaakov, H., Ankri, L., Mayzel, J., Gilead, N.,
1095 Parness-Yossifon, R., Rivlin-Etzion, M. (2022). Top-down modulation of the retinal code
1096 via histaminergic neurons of the hypothalamus. bioRxiv, 2022.04.26.489509.

1097 Warwick, R.A., Riccitelli, S., Heukamp, A.S., Yaakov, H., Swain, B.P., Ankri, L., Mayzel,
1098 J., Gilead, N., Parness-Yossifon, R., Di Marco, S., Rivlin-Etzion, M. (2024). Top-down
1099 modulation of the retinal code via histaminergic neurons of the hypothalamus. Sci Adv.
1100 10(35):eadk4062.

1101 White, J.M., Rumbold, G.R. (1988). Behavioural effects of histamine and its antagonists:
1102 a review. Psychopharmacology (Berl) 95(1), 1-14.

1103 Wilson, M., Lindstrom, S.H. (2011). What the bird's brain tells the bird's eye: the function
1104 of descending input to the avian retina. Vis Neurosci, 28(4), 337–350.

1105 Yu, Y., Satoh, H., Wu, S.M., Marshak, D.W. (2009). Histamine enhances voltage-gated
1106 potassium currents of ON bipolar cells in macaque retina. Invest Ophthalmol Vis Sci, 50(2),
1107 959–965.

1108 Yu, Y., Satoh, H., Vila, A., Wu, S.M., Marshak, D.W. (2011). Effects of Histamine on Light
1109 Responses of Amacrine Cells in Tiger Salamander Retina. Neurochem Res, 36, 645–654.

1110 Yu, X., Ye, Z., Houston, C.M., Zecharia, A.Y., Ma, Y., Zhang, Z., Uygun, D.S., Parker, S.,
1111 Vyssotski, A.L., Yustos, R., Franks, N.P., Brickley, S.G., Wisden, W. (2015). Wakefulness
1112 Is Governed by GABA and Histamine Cotransmission. Neuron, 87(1), 164–178.

1113 Yüzgeç, Ö., Prsa, M., Zimmermann, R., Huber, D. (2018). Pupil size coupling to cortical
1114 states protects the stability of deep sleep via parasympathetic modulation. Curr Biol 28,
1115 392–400.e3.